Innovative Infrastructure Solutions (2026) 11:192
https://doi.org/10.1007/s41062-026-02587-0

TECHNICAL PAPER

A dynamic lane activation control system for the intelligent and self-regulating COM-Roundabout

Marco Guerrieri[1] · **Masoud Khanmohamadi**[1]

Received: 10 December 2025 / Accepted: 22 February 2026

Abstract

This study proposes a dynamic lane-control strategy for the novel smart and self-regulating COM-Roundabout, which simultaneously optimizes capacity, safety, and performance under the emergent effects of connected and automated vehicles (CAVs). The proposed model integrates specific capacity and delay models (from the HCM manual) and crash-prediction relationships (from the NCHRP 888 Report) and CAV-specific capacity adjustment factors within a unified optimization platform. Since COM-Roundabout allows the adoption of very different scenarios by activating and deactivating entry and circulating lanes, a dynamic system was considered using one-hour control intervals. The proposed optimization controller balances delays and crash risk while imposing penalties on unnecessary lane switches. Its performance was tested across 5,000 synthetic traffic demand profiles. Compared with a single-lane baseline, the dynamic scenario reduces mean delays by more than half, while avoiding most of the safety penalties associated with permanent scenarios. Parametric analyses reveal piecewise regime transitions in the delay–safety trade-off that arise from discrete changes in lane-activation states selected by the controller. Higher CAV penetration further magnifies the gains by accelerating congestion relief. Overall, the study demonstrates that dynamic per-arm lane control offers a feasible and transitional strategy for delivering safer and more efficient roundabout operations in an era of smart roads and intersections.

Keywords Smart roundabouts, COM-Roundabout · Dynamic lane control system · Managed lane strategies · Safety-capacity trade-off

List of symbols

A	Configuration-specific regression parameter of the entry capacity formula
$AADT_{ij}$	Annual average daily traffic for the stream component *i-j*
Ac	Active lane
$ApprAADT_i$	Average total daily entering flow to the roundabout from leg *i*
B	Configuration-specific regression parameter of the entry capacity formula
C	Total roundabout capacity (veh/h)
c_i	Entry capacity of the arm *i* (veh/h)
CAVs	Connected and automated vehicles
CMFs	Crash modification factors
CCTV	Closed-circuit television
$CircAADT_i$	Average total daily circulating flow in front of the entry *i*
$C(s)$	Total capacity of the entire roundabout under the configuration *s* (veh/h)
d	Mean delay at the whole roundabout (s)
d_l	Control delay of the lane l (s/veh)
$d(s)$	Average control delay at the whole roundaboutrelated to the slot duration (s/veh)
$E(s)$	Expected crashes per hour at the whole roundabout related to the slot duration (crashes/h)
E_i	Expected total crashes on leg *i* (crashes/year)
$E_{i,slot}$	Expected number of crashes during each control slot (crashes/year)
f_A	First capacity adjustment factor to reflect the CAVs proportion in the traffic flow
f_B	Second capacity adjustment factor to reflect

✉ Marco Guerrieri
marco.guerrieri@unitn.it

[1] Department of Civil, Environmental and Mechanical Engineering (DICAM), University of Trento, Via Mesiano 77, 38123 Trento, Italy

Published online: 25 March 2026

	the CAVs proportion in the traffic flow
$f(\pi_i)$	Dirichlet density function
HDVs	Human-driven vehicles
I	Inactive lane
I_{change}	Binary indicator
LOS	Level of service
$p_{ij}(t)$	Probability that a vehicle entering at arm i exits at arm j
PHF	Peak-hour factor
Q_{l}	Queue of the lane l (veh)
$q(t)$	Inflow vector (veh/h)
$Q_{i,j}(t)$	Volume that enters at arm i of the roundabout and exits from arm j (veh/h)
$q_{c,i}$	Circulating flow in front of the arm i (veh/h)
q^{base}	Typical hourly traffic demand under normal, non-congested conditions
q^{peak}	Maximum hourly traffic demand assumed during peak hours
SPFs	Safety performance functions
t_c	Users' critical headway (s)
t_f	Users' follow-up time (s)
V2I	Vehicle to infrastructure communication system
V2V	Vehicle to vehicle communication system
w_{delay}	Normalized weighting factors for delay
w_{safety}	Weighting factors for safety
x	Degree of saturation
α_k	Ratio of design hourly volume to AADT
α_k	k-th Dirichlet concentration/shape parameter
α^{arm}	Dirichlet parameter vector is used to split the total design-hour demand across the four arms
α_0	Sum of Dirichlet parameters
η	Switching penalty coefficient
π_i	Fraction (share) of total demand assigned to arm i

Introduction

Roundabouts are widely recognized for improving safety and reducing delays relative to conventional intersections. Recent research shows that converting stop-controlled or signalized intersections to single-lane roundabouts can significantly cut total crashes [1–3]. These benefits have led to widespread adoption among road networks, above all in urban contexts. Despite these benefits, the roundabout can still experience highly delays in the event of increased demand for capacity or severe inflow imbalances. However, designing a roundabout requires balancing conflicting objectives: the entrance width and number of circulating lanes are the primary determining factors of capacity, yet wider entrances and circulating lanes with turning widths are often associated with a higher frequency of crashes [4]. To maximise safety, international design guidelines generally recommend keeping entries as narrow as practicable and using flaring or staged expansions to provide capacity only when needed. This has motivated a line of research into adaptive control and geometric design improvements of roundabouts. The novel COM-Roundabout concept (Fig. 1), examined in this research, integrates vehicle detectors, smart cameras, LED road markers, and variable message signs to dynamically adjust the number of active entry and circulating lanes based on measured traffic demand [5], thereby optimizing safety and functional performance. By evaluating capacity, delay, level of service, and predicted crashes across many traffic scenarios using HCM and Highway Safety Manual models, this smart and self-regulating roundabout demonstrates that dynamic lane assignments can optimize its performance in real-time. Recent studies have highlighted the growing importance of real-time, network-level delay estimation using passive detection and turning-movement-based input–output formulations as a foundation for advanced adaptive traffic control systems [6]. Existing operational forecast methods, such as those in the HCM, prescribe capacity and delay formulas for single-lane and two-lane conventional roundabouts, typically analyzing the road intersection under a fixed (uniform) lane configuration [7]. Several safety models are available in scientific literature. Among these models. The NCHRP Research Report 888 proposes safety performance functions (SPFs) and crash modification factors (CMFs) that incorporate traffic volumes, geometric features, and lane counts for roundabouts [8]. Still, these models assume static lane configurations and cannot adjust to time-varying demand because they were obtained by analyzing conventional roundabouts. Dynamic lane assignment on freeways offers a useful analogy for better understanding the benefits of the smart and self-regulating COM-Roundabout. Managed-lane strategies, such as reversible lanes, dynamic merge control, and hard-shoulder running systems, repurpose road space based on prevailing, expected or current traffic demand, improving operational performance and safety without permanently adding capacity [9, 10]. In this paradigm, dynamic lane assignment reallocates available lanes to specific traffic streams to use existing infrastructure more efficiently and safely and at lower cost than constructing new lanes; implementation typically relies on static or electronic lane-control signs and, where applicable, movable barriers, supported by detection sensors, software, Closed-Circuit Television (CCTV), and inter-agency coordination [10, 11]. These principles motivate dynamic lane control for roundabouts, wherein the same geometric infrastructure can operate in one-lane or two-lane mode on individual approaches

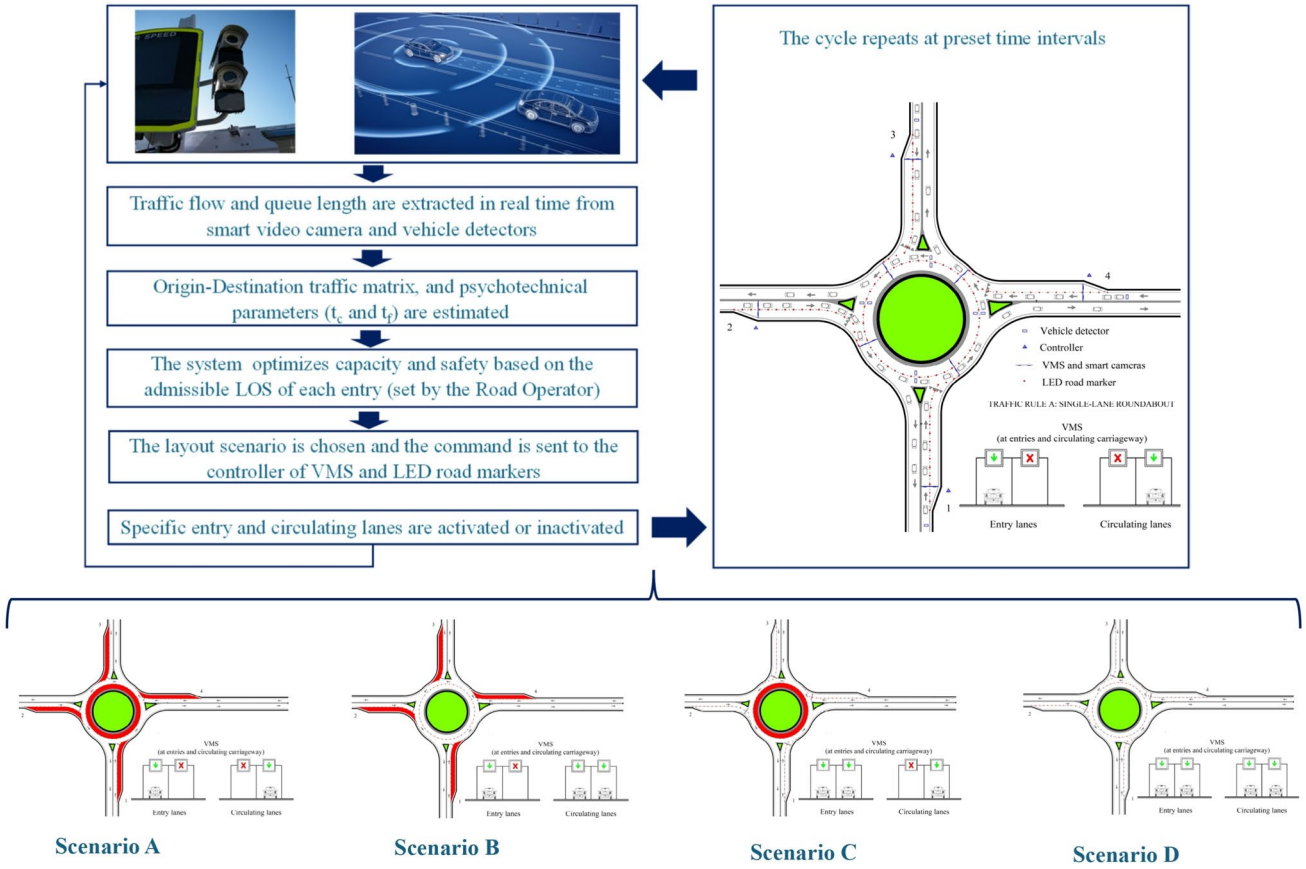

Fig. 1 System architecture and control loop for dynamic per-arm lane control (COM-Roundabout) with the main four scenarios analyzed in the research

in response to real-time demand and safety conditions [11, 12]. In addition, the emergence of connected and automated vehicles adds a new dimension to roundabout management. Cooperative adaptive cruise control allows CAVs to accept shorter gaps and follow more closely than human-driven vehicles (HDVs), potentially increasing entry capacity and smoothing flow. The HCM 7th edition, introduced CAV capacity-adjustment factors for several road elements, including roundabouts; these factors modify the exponential capacity equations to reflect the presence of CAVs [7]. At high penetration levels, CAVs substantially enhance traffic flow stability, leading to increases in roundabout capacity. Simulation evidence suggests that automation can reduce stop-and-go waves and improve travel time reliability [13]. Because level-4/5 CAVs are not yet common in practice, these factors are derived from simulations under the assumption of reliable vehicle to vehicle (V2V) and vehicle to infrastructure (V2I) communications [14]. Simulation models of CAVs often assume perfect, delay-free communication between vehicles and infrastructure. While this assumption supports controlled evaluations, it may overestimate performance compared with real-world deployments [15]. Microsimulation studies have shown that introducing CAVs can significantly reduce surrogate safety conflicts at conventional and unconventional roundabouts, particularly under mixed traffic conditions [16]. While microscopic simulations have demonstrated that increasing CAV penetration rates significantly reduces the frequency of dangerous situations and improves time-to-collision distributions, leading to smoother traffic flow and enhanced traffic safety in mixed traffic conditions [17]. Advanced CAV models integrate both onboard sensing and V2V communication to perceive the environment and predict traffic states. These studies generally treat communication as highly reliable, which simplifies analysis but diverges from current technological limitations [18]. Incorporating these CAV adjustments enables researchers to investigate the interaction between dynamic lane control and technology adoption.

Recent research on dynamic lane-use strategies and active traffic management has expanded beyond traditional freeway applications and increasingly targets corridor- and intersection-level efficiency gains using real-time detection, lane-control signals, and adaptive rules. Guidance and syntheses on dynamic lane-use control within active traffic management frameworks highlight the operational rationale and field implementation requirements (detection, lane-control

signing, and hold-time logic) [12, 19]. In parallel, simulation-based studies continue to investigate dynamic lane assignment and lane reversal strategies in urban contexts, showing that adaptive lane allocation can reduce congestion under peak and directional imbalance traffic conditions [20, 21]. Regarding automation, recent work on mixed CAV/HDV behaviour in roundabouts confirms that penetration rate and interaction rules can materially change roundabout performance [22, 23], while safety assessment under automation often relies on microsimulation and surrogate safety indicators due to limited crash data for high-automation regimes [24, 25]. These trends motivate the proposed COM-Roundabout controller as an intersection-scale dynamic lane-use strategy that unifies operational performance and safety under a single decision framework.

This study presents a dynamic lane control framework for each arm at COM-Roundabout and broadens managed lane principles beyond traditional freeway uses. A lane-level analytical model combines capacity relationships from the HCM with formulas for control delay, queue length, and level of service (LOS). To capture automation effects, HCM capacity-adjustment factors scale entry-capacity curves across varying penetration rates of connected and autonomous vehicles in the total flow. Safety is explicitly incorporated using leg-level crash prediction functions from NCHRP Report 888. The control problem is formulated as a dynamic optimization where up to two lanes can be assigned to each entry arm and the circulatory lane. This results in a finite set of 32 feasible lane configurations (Table 1). The objective function merges normalized control delay and predicted crash frequency into a weighted performance indicator, subject to a recovery rule that requires restoring any approach with LOS F to LOS B or better in the next control step. To prevent oscillations in lane assignments, a switching penalty is applied when configurations are changed. The 12-h planning horizon considered in the research is divided into hourly control slots, each representing a decision period during which demand and capacity are assumed to be in approximately steady-state conditions. At the beginning of each time interval, the controller updates the traffic situation based on the latest data and selects an optimal lane assignment that remains constant for the entire hour. This formulation allows for gradual adaptation of the field geometry while ensuring operational stability and computational routing capability. Traffic demand levels for roundabout functional and safety evaluation are generated through a two-level Dirichlet process with acceptance sampling, producing diverse origin–destination $M_{O/D}$ traffic matrices that capture both directional flows imbalance and peak formation. Time-varying traffic demand profiles further reflect realistic fluctuations. performance of the dynamic controller is benchmarked against static one-lane and two-lane roundabout designs using multiple operational and safety metrics. Sensitivity analyses examine the impact of varying weightings between delay and crash minimization, while a schedule plot illustrates the temporal progression of lane allocations. Finally, practical considerations such as driver communication, detection requirements, and public acceptance are discussed in the context of real-world deployment.

Objectives and limitations of the research

In summary, the main innovations and contributions of this article are as follows:

Table 1 Possible scenarios of the COM-Roundabout, depending on the active and inactive lanes at entries and on the ring (Ac = active, I = inactive)

One circulating lane Second entry lane					Two circulating lanes Second entry lane				
Scenario	Arm 3	Arm 2	Arm 3	Arm 4	Scenario	Arm 1	Arm 2	Arm 3	Arm 4
S1	I	I	I	I	S17	I	I	I	I
S2	Ac	I	I	I	S18	Ac	I	I	I
S3	I	Ac	I	I	S19	I	Ac	I	I
S4	I	I	Ac	I	S20	I	I	Ac	I
S5	I	I	I	Ac	S21	I	I	I	Ac
S6	Ac	Ac	I	I	S22	Ac	Ac	I	I
S7	Ac	I	Ac	I	S23	Ac	I	Ac	I
S8	Ac	I	I	Ac	S24	Ac	I	I	Ac
S9	I	Ac	Ac	I	S25	I	Ac	Ac	I
S10	I	Ac	I	Ac	S26	I	Ac	I	Ac
S11	I	I	Ac	Ac	S27	I	I	Ac	Ac
S12	Ac	Ac	Ac	I	S28	Ac	Ac	Ac	I
S13	Ac	Ac	I	Ac	S29	Ac	Ac	I	Ac
S14	Ac	I	Ac	Ac	S30	Ac	I	Ac	Ac
S15	I	Ac	Ac	Ac	S31	I	Ac	Ac	Ac
S16	Ac	Ac	Ac	Ac	S32	Ac	Ac	Ac	Ac

a. describe the main technical characteristic of the novel COM-Roundabout;
b. proposed closed-form models able to estimate capacity, delay, level of service and accidents of the COM-Roundabout in different layout scenarios;
c. studying the traffic effect on the COM-Roundabout capacity and safety generated by the variation of layout configuration in terms of active and inactive lanes;
d. examining how different percentages of CAVs in traffic flows could influence the performance of the system in terms of capacity and delay.

This research is subject to certain limitations that arise at various phases of the analysis. The most significant constraint is that the COM-Roundabout is still at a conceptual design stage; consequently, the analysis relies exclusively on closed-form capacity models traditionally adopted for conventional roundabouts. Moreover, only light vehicle traffic was considered. The study does not address transient traffic conditions or incorporate stochastic driver behaviour models. Lastly, the safety effect related to the CAVs presence is not considered.

The rest of the paper is structured as follows. Sect. "Methodology" describes the methodology used to estimate the traffic performance of the COM-Roundabout in terms of capacity and safety, with a specific focus on the Dynamic Lane Control Optimisation system. Results and Discussion are given in Sect. "Results and discussion". Sect. "Discussion" focuses on the results discussions. Finally, Sect. "Conclusions" presents the conclusions, the study's limitations, and research perspectives.

Methodology

In this work, the roundabout under consideration (i.e. the COM-Roundabout) is no longer conceived as a fixed physical infrastructure but as an adaptive traffic management system capable of responding to real-time traffic conditions. The conceptual framework, depicted schematically in Fig. 1, is a closed-loop process comprising sensing, estimation, optimization, and actuation. Data on approach flows, queue lengths and circulating volumes are gathered continuously from inductive loop detectors and intelligent cameras positioned upstream of each entry. These data streams underpin the estimation of the current origin–destination traffic matrix and the parameters of driver behavior, notably the critical gap and the follow-up time. These estimates feed directly into the optimization module, where established HCM formulations are used to compute entry capacities, delays and queue lengths, while safety is assessed through crash prediction functions from NCHRP Report 888. In this study, the term controller refers to the decision mechanism that selects the optimal lane-configuration state at each time step based on the evaluated operational and safety performance. At fixed one-hour intervals, the controller evaluates every feasible lane configuration and selects the one that minimizes a weighted sum of normalized delay and expected crashes. To prevent rapid oscillations in lane assignments, a switching penalty is introduced. Conversely, a recovery rule ensures that any arm operating at a level of service LOS F is expanded with the activation of the additional lane until at least level LOS B is achieved. Once the optimal configuration has been determined, the actuation stage conveys lane assignments to road users. Variable message signs and embedded LED lane markers clearly indicate which entry and circulating lanes are open. In a cooperative automated vehicle environment, these instructions can be transmitted directly to CAVs, allowing automated lane selection and trajectory control. The cycle then repeats for the next time slot, allowing the roundabout to adjust continuously to temporal and spatial variations in arriving flows (i.e. in function of the traffic demand). This flexible architecture gives rise to a rich set of operational modes. The selection of control delay, degree of saturation (v/c), and level of service (LOS) as primary performance indicators follows established inflection-based degradation analysis frameworks, where intersection performance is evaluated over long-term demand growth to identify operational tipping points requiring geometric or control intervention [26]. Each approach may operate with one or two entry lanes, while the circulatory lane may be single- or dual-lane and it is independent of the entriy configurations. The combination of these possibilities yields 32 distinct lane-activation scenarios, summarized concisely in Table 1. In Table 1, an active lane is denoted by 'Ac' and an inactive lane by 'I'. Scenario S1 corresponds to the most conservative configuration, single-lane approaches and a single circulating lane, mirroring a conventional single-lane roundabout. At the opposite extreme, Scenario S32 activates all entry and circulating lanes, replicating the behavior of a conventional two-lane roundabout. Between these limits lie a continuum of intermediate configurations in which one or more arms are selectively upgraded while others remain single-lane, allowing the system to target additional capacity where it is most needed and to avoid unnecessary exposure to the higher crash risks associated with fully multilane operation. Together, Fig. 1 and Table 1 encapsulate the operational logic of the COM-Roundabout. More precisely, Fig. 1 illustrates the real-time sensing–estimation–optimization–actuation loop that governs system behavior, while the table enumerates the full spectrum of lane-activation states available to the controller. Their integration demonstrates how the roundabout can evolve from a static piece of infrastructure into a self-regulating system capable of

dynamically balancing efficiency and safety. The proposed methodology, in brief, is based on the following process. The COM-Roundabout has a certain initial layout at time t, relative to one of the scenarios indicated in Table 1. Traffic demand for time t is generated in terms of the origin–destination matrix $M_{O/D}(t)$. Capacity, delays, LOS, and accident rates are calculated. The optimization algorithm is then applied to obtain the desired combination of traffic performance and safety requested by the manager operator. This information is transmitted to the traffic control system, and the roundabout layout is modified accordingly. The procedure is then iterated at time $(t+\Delta t)$, when traffic conditions change according to the new origin–destination matrix $M_{O/D}(t+\Delta t)$. In parallel, the proposed method evaluates the effects of the presence of CAVs on capacity, delays, and LOS. The procedure is explained in detail in the following subsections.

Traffic demand generation

To evaluate the performance and safety of the COM-Roundabout under different available scenarios (cf. Table 1), extensive traffic simulations were conducted with the assumption that circulating and exit lanes remained undersaturated (x=flow/capacity<1), so any congestion could only arise from saturated entries. Transient conditions were not considered in this study. At each time step t, the traffic demand is represented by a 4×4 origin–destination matrix $M_{O/D}(t)$ (see Eq. (1)) whose element $Q_{i,j}(t)$ denotes the volume (veh/h) that enters at arm i and exits at arm j:

$$M_{O/D}(t) = \begin{vmatrix} Q_{1,1}(t) & Q_{1,2}(t) & Q_{1,3}(t) & Q_{1,4}(t) \\ Q_{2,1}(t) & Q_{2,2}(t) & Q_{2,3}(t) & Q_{2,4}(t) \\ Q_{3,1}(t) & Q_{3,2}(t) & Q_{3,3}(t) & Q_{3,4}(t) \\ Q_{4,1}(t) & Q_{4,2}(t) & Q_{4,3}(t) & Q_{4,4}(t) \end{vmatrix} \quad (1)$$

The conventional number assigned to arms is given in Fig. 1.

Equation 1 may be written compactly as a vector $[Q_{ij}(t)]$ for i,j=1,2,3,4. Heterogeneous traffic demand was modeled using origin–destination matrices sampled from Dirichlet distributions, which provide flexible and statistically consistent turning proportions of flows across all approaches. For example, for entry 1 in Scenario a (a single-lane entry conflicting with one circulating lane, cf. Fig. 1), the circulating flow at time t is:

$$\begin{aligned} q_{c,1}(t) = {} & (Q_{2,4}(t) + Q_{2,3}(t) + Q_{2,2}(t)) \\ & + (Q_{3,4}(t) + Q_{3,3}(t)) + Q_{4,4}(t) \end{aligned} \quad (2)$$

and the entry flow is $q_{e,1}(t)=Q_{1,1}(t)+Q_{1,2}(t)+Q_{1,3}(t)+Q_{1,4}(t)$; the entry capacity and control delay are then obtained from Eqs. (4) to (12). In this research it was assumed that the hourly volumes are related to the annual average daily traffic (AADT) via the relation:

$$Q_{ij} = \alpha \cdot PHF \cdot AADT_{ij} \quad (3)$$

where α (typically 0.08–0.10) represents the ratio of design hourly volume to AADT, and PHF is the peak-hour factor (0.90–0.95 on urban roads).

Each experiment considered the four-leg roundabout depicted in Fig. 1 over a 12-h horizon, subdivided into 60-min control intervals. To capture temporal variation, time-dependent arrival rates on each approach were generated using Gaussian-shaped demand profiles, reproducing the build-up and dissipation of a mid-day traffic peak. For each realization, origin–destination flows were scaled to yield an AADT between 20,000 and 80,000 veh/day, then converted to design-hour flows using α=0.10 and PHF=0.90. To ensure realistic and comparable simulation conditions, a rejection step excluded any scenarios in which the maximum control delay exceeded 100 s/veh, representing excessively congested and practically unrealistic operations, or where more than 30% of intervals operated at LOS F. The latter threshold was specifically introduced to ensure that Scenario A (cf. Fig. 1), serving as the base case, maintained a moderate level of congestion, approximately 30% LOS F, thereby allowing the subsequent scenarios (B–D and the dynamic configuration) to demonstrate measurable performance improvements. This ensured that comparisons among scenarios remained meaningful from both safety and operational perspectives, and that the dynamic policy faced realistic trade-offs between delay and safety. Although 32 different roundabout configurations can be implemented as summarized in Table 1, for simplicity's sake, only the following 4 have been considered in this research:

- Scenario A—single entry and single circulatory lane on all legs;
- Scenario B—two entry lanes, one circulatory lane;
- Scenario C—single entry lane, two circulatory lanes; and
- Scenario D—two entry and two circulatory lanes.

These four scenarios are schematized in Fig. 1. The study then considered a dynamic scenario, in which the COM-Roundabout can change its configuration over time, alternating among the four scenarios listed above based on the current traffic demand at time slot t. Although 32 feasible lane-activation configurations are theoretically available (Table 1), four representative configurations (Scenarios A–D) are selected as static benchmark designs for comparative purposes, because they correspond to conventional single- and two-lane roundabout layouts commonly

analyzed in practice. These four scenarios are used only as fixed reference designs. In contrast, the dynamic controller evaluates all 32 feasible lane-activation configurations at every control slot and may select any of them as the optimal operating state. The present analytical framework assumes that circulating and exit lanes remain undersaturated (x < 1) and that traffic conditions within each one-hour control slot can be approximated as steady state. As a result, transient queue spillback, exit blocking, shockwave propagation, and time-to-clear dynamics are not explicitly represented. This modeling envelope reflects the intended operational domain of intersection-scale lane-activation control under moderately to heavily loaded—but still functional—roundabout conditions. Under extreme oversaturation, where spillback and unstable shockwave behavior dominate, microsimulation or network-level control strategies would be required, and the present analytical formulation would no longer be sufficient.

Measure of effectiveness: capacity and delay estimation

Capacity is a fundamental traffic parameter in the design and analysis of transportation facilities, particularly at roundabouts, where it underpins measures of effectiveness such as delay, queue length, and level of service.

Scholars have noted that capacity itself can be described in several ways, including entry capacity, simple capacity and total capacity [27, 28]. Both simple and total capacities ultimately depend on the entry capacity, which is usually estimated with gap-acceptance models such as those found in the current HCM. In these models, the capacity of a particular entry is treated as a function of the circulating flow, the critical headway for the subject entry, and the follow-up time required between vehicles. For the generic approach i, the entry capacity c_i (vehicles per hour) depends on the opposing circulating flow $q_{c,i}$ and the psychotechnical parameters, critical headway t_c and follow-up time t_f. This dependence is encapsulated by the Siegloch exponential model [7]:

$$c_i = Ae^{-B \cdot q_{c,i}} \tag{4}$$

$$A = \frac{3600}{t_f} \tag{5}$$

$$B = \frac{t_c - \frac{t_f}{2}}{3600} \tag{6}$$

where A and B are configuration-specific regression parameters. The HCM provides calibrated A and B values for different numbers of entry and circulating lanes. Table 2 summarizes the four primary lane combinations and their resulting capacities. When two entry lanes are active, the approach capacity is [8]:

$$c_i = \frac{c_{i,R} + c_{i,L}}{max\left(\frac{q_{e,i,R}}{c_{i,R}}; \frac{q_{e,i,L}}{c_{i,L}}\right)} \tag{7}$$

in which the symbols L and R in each traffic variable indicate the left and right lane of the entry i, respectively. More precisely, $q_{e,i,R}$ and $q_{e,i,L}$ are the entering flows from the right lane and left lane of the arm i, respectively; instead, $c_{i,R}$ and $c_{i,L}$ are the corresponding capacities. The total roundabout capacity is obtained as $C = \sum_{i=1}^{N} c_i$. The critical headway t_c and follow-up time t_f may vary by approach and are updated from detector data of the COM-Roundabout, but the exponential form above is maintained. The t_c and t_f play a crucial role in determining entry capacity. Although they are commonly estimated from traffic data and treated as fixed values, these parameters vary with driver behavior, traffic composition, and temporal conditions. Such variability can cause significant fluctuations in entry capacity and lead to inaccurate performance or LOS assessments if static values are assumed. Conversely, in COM-Roundabouts, t_c and t_f can be estimated in real time, and therefore, the capacities can be calculated realistically. The volume–capacity ratio (i.e. the degree of saturation) of a lane l is defined as x = q/c. Control delay d_l (in seconds per vehicle) of the generic entry lane is computed using the HCM delay formula [7]:

$$d_l = \frac{3600}{c} + 900 \cdot T \cdot \left[x - 1 + \sqrt{(x-1)^2 + \frac{\frac{3600}{c} \cdot x}{450 \cdot T}}\right] + 5 \cdot min[x, 1] \tag{8}$$

where T is the time interval period.

The 95th-percentile queue length is obtained from a similar expression with different constants [7]:

$$Q_l = 950 \cdot T \cdot \left[x - 1 + \sqrt{(x-1)^2 + \frac{\frac{3600}{c} \cdot x}{150 \cdot T}}\right] \cdot \left(\frac{c}{3600}\right) \tag{9}$$

Table 2 Empirical HCM capacity equations for different entry and circulating-lane configurations at roundabouts [7]

Configuration (cf. Figure 1)	Description	Entry capacity equation
Scenario A	1 entry lane and 1 circulating lane	$c_i = 1380e^{(-1.02 \cdot 10^{-3}) \cdot q_{c,i}}$
Scenario B	2 entry lanes and 1 circulating lane	$c_i = 1420e^{(-0.91 \cdot 10^{-3}) \cdot q_{c,i}}$
Scenario C	1 entry lane and 2 circulating lanes	$c_i = 1420e^{(-0.85 \cdot 10^{-3}) \cdot q_{c,i}}$
Scenario D	2 entry lanes and 2 circulating lanes	Right: $c_{i,R} = 1420e^{(-0.85 \cdot 10^{-3}) \cdot q_{c,i}}$ Left: $c_{i,L} = 1350e^{(-0.92 \cdot 10^{-3}) \cdot q_{c,i}}$

Table 3 Level of service (LOS) as a function of control delay [7]

Control delay [s/veh]	Level of service (LOS)	
	x = volume/capacity ≤ 1	x = volume/capacity > 1
0–10	A	F
10–15	B	F
15–25	C	F
25–35	D	F
35–50	E	F
> 50	F	F

In the case of activation of two lanes, the flow is split into right and left lanes in the proportion (50/50). This represents a neutral and analytically convenient baseline that avoids introducing site-specific lane-use rules, pavement marking schemes, or driver preference parameters that are not yet standardized for COM-Roundabout deployments. It should be noted, however, that real-world lane utilization is often turning-dependent and context-specific [29]. Non-uniform lane splits may therefore shift absolute delay and crash estimates, particularly under heavy demand. Nevertheless, the relative comparison between static and dynamic configurations is preserved, because the same lane-split assumption is applied consistently across all evaluated scenarios. The delay and capacity for each lane are computed separately and then combined. The approach delay is the demand-weighted average of lane delays (Eq. 10).

$$d_i = \frac{d_{e,i,R} \cdot q_{e,i,R} + d_{e,i,L} \cdot q_{e,i,L}}{q_{e,i,R} + q_{e,i,L}} \tag{10}$$

The mean delay d at the whole roundabout is obtained by weighting arm delays by their entering flows (Eq. 11) [7]:

$$d = \frac{\sum_{i=1}^{N} d_i \cdot q_{e,i}}{\sum_{i=1}^{N} q_{e,i}} \tag{11}$$

Levels of service (LOS) A–F are assigned based on control-delay thresholds given in Table 3.

Safety model

At each control interval, the traffic control system allows the use of one or two lanes on each leg and on the ring. The expected crash frequency for each leg of the COM-Roundabout is estimated using the leg-level Safety Performance Functions (SPFs) of the NCHRP Research Report 888 [8] developed for conventional roundabouts. These SPFs were calibrated from U.S. roundabout crash data and predict the annual number of crashes on a single approach as a function of traffic volumes, lane configuration and rural/urban context.

Table 4 Estimated parameters for the leg-level crash prediction model—single circulating lane [8]

Variable	Parameter	Estimate (standard error)
Intercept	a	−10.5458 (1.1847)
Approach AADT	b	0.8197 (0.0929)
Circulating AADT	c	0.2747 (0.0657)
Rural area indicator	d	0.3673 (0.1820)
Two entering lanes	e	0.9827 (0.1536)

For a single circulating lane, the expected total number of crashes per year on leg i is given by:

$$E_i = exp^{a} ApprAADT_i^{b} CircAADT_i^{c} \; exp^{(d \times AreaType_i + e \times TwoEnteringLanes_i)} \tag{12}$$

where:

E_i is the expected total crashes on leg i (crashes/year);

$ApprAADT_i$ is the average total daily entering flow to the roundabout from leg i;

$CircAADT_i$ is circulating AADT (veh/day), representing the daily circulating flow immediately upstream of the leg i;

$AreaType_i$ is a binary variable (0 for urban, 1 for rural) identifying the surrounding area type;

$TwoEnteringLanes_i$ is the indicator variable equal to 1 if the approach has two entry lanes, and 0 otherwise;

$TwoExitingLanes_i$ is the indicator variable equal to 1 if the exit has two exit lanes, and 0 otherwise;

a, b, c, d, e are regression coefficients.

For two circulating lanes, the expected total crashes per year on leg i are:

$$E_i = exp^{a} ApprAADT_i^{b} CircAADT_i^{c} \; exp^{(d \times AreaType_i + e \times TwoEnteringLanes_i + f \times TwoExitingLanes_i)} \tag{13}$$

where $TwoEnteringLanes_i$ is 1 if the exit has two lanes and 0 otherwise and f is its regression coefficient. Tables 4 and 5 provide the calibrated parameters a, b, c, d, e and f for the total-crash SPFs defined in Eqs. (12) and (13). These coefficients should not be applied to other crash-type-specific models.

Note that Eqs. (12) and (13) are total-crash Safety-Performance Functions. The coefficients reported in Tables 4 and 5 were calibrated from NCHRP 888 for the total crash frequency at each leg; consequently, these formulas predict the expected overall number of crashes (combining all collision types and severity levels). They are therefore applicable when estimating total roundabout-crash risk rather than individual crash types. These safety-performance functions are applied separately to each approach, with the

Table 5 Estimated parameters for the leg-level crash prediction model—two circulating lanes [8]

Variable	Parameter	Estimate (standard error)
Intercept	a	−7.1029 (1.6107)
Approach AADT	b	0.4443 (0.1039)
Circulating AADT	c	0.3306 (0.1421)
Rural area indicator	d	0.4194 (0.2393)
Two entering lanes	e	0.2950 (0.1381)
Two exiting lanes	f	0.3805 (0.1139)
Overdispersion parameter	k	0.9429 (0.1437)

expected crash frequency determined by a combination of the approach and circulating traffic volumes and a set of indicator variables for geometric and contextual factors. The model structure incorporates diminishing marginal effects of traffic exposure through the logarithmic–power terms, while the area type and the presence of two entering lanes influence the prediction through multiplicative adjustment factors. Because NCHRP 888 defines all SPFs at the leg level, each approach can be evaluated according to its own characteristics, even when different legs of the same roundabout have different numbers of lanes or geometric features. The total roundabout-level expected crashes are obtained by summing the approach-level estimates.

In this study, the corresponding equation (single-lane or two-lane) was applied independently to each leg according to its instantaneous lane configuration, based on the scenario present at time t. Finally, to obtain the expected number of crashes during each control slot $E_{i,slot}$, the annual value E_i was scaled by the slot duration T_{slot} (in hours) and divided by the total number of hours in a year (8,760 h):

$$E_{i,slot} = E_i \frac{T_{slot}}{8760} \tag{14}$$

This transformation ensures consistency between the safety estimates and the one-hour operational intervals used in the traffic simulation. These leg-level SPFs have been widely validated and adopted in North American practice for safety evaluation of roundabouts, providing a robust and empirically grounded measure of expected crash frequency under varying traffic and geometric conditions.

Dynamic lane control optimization

The dynamic control problem is formulated over a finite prediction horizon consisting of N discrete control slots (each lasting one hour in this study). At every time slot t, the system occupies a state st that defines the number of entry lanes on each approach (either one or two) and the number of circulatory lanes (also either one or two). The vector of entering flows in the whole roundabout, denoted as $q(t) = [q_1(t), q_2(t), q_3(t), q_4(t)]$, represents the total approach flow rates (veh/h) entering the roundabout from each arm. These values are directly derived from the $Q_{i,j}$ component flow of the origin–destination traffic matrix , which specifies the demand from each origin approach i to each destination exit j. q_i is the total flow entering from the generic arm i, therefore, it is obtained as follows:

$$q_i(t) = \sum_{j=1}^{4} Q_{ij}(t) \tag{15}$$

For a given state s the following variables and notation are considered:

- C(s) denotes the total capacity of the entire roundabout (veh/h), expressed as the sum of the entry capacities under the configuration s;
- d(s) represents the average control delay per vehicle (s/veh) at the whole roundabout level, computed as the demand-weighted mean of approach delays;
- E(s) is the expected crashes per hour (crashes/h) for the same configuration, obtained by summing the leg-level crash predictions from the safety model (Sect. "Safety model") and scaling them by slot duration.

To determine the optimal configuration (i.e. the optimal scenario) of the COM-Roundabout at each slot, a multi-objective cost function is considered as follows:

$$J(s) = w_{delay}\frac{d(s) - d_{min}}{d_{max} - d_{min}} + w_{safety}\frac{E(s) - E_{min}}{E_{max} - E_{min}} + \eta I_{change} \tag{16}$$

where:

- *J(s)* is a dimensionless objective function that quantifies the overall performance cost of state s; lower values indicate better performance;
- w_{delay} and w_{safety} are normalized weighting factors for delay and safety, respectively, satisfying the condition $w_{delay}+w_{safety}= 1$. This ensures that the two components jointly express a relative trade-off between operational efficiency and crash risk, rather than absolute magnitudes with inconsistent units:
- *E(s)*, E_{min}, and E_{max} are defined analogously for expected crashes (crashes/h);
- η is the switching penalty coefficient, typically set to a small positive value (e.g., 0.0–0.1), that discourages unnecessary lane changes between consecutive slots;
- I_{change} is a binary indicator equal to 1 if the selected state differs from the previous slot's configuration and 0 otherwise.

The optimization is performed over the full set of 32 feasible lane-activation states, whereas Scenarios A–D are used solely as static benchmark layouts for performance comparison. At each control slot, the dynamic controller evaluates every feasible lane-state configuration (one lane or two lanes on each approach, and for one or two circulating lanes) and computes its mean delay, d(s). At each control slot, d_{min} is defined as the smallest mean delay among all feasible lane-state configurations s, and d_{max} is defined as the largest mean delay among those configurations. Both reference values are recalculated every hour because they depend on the prevailing inflow and the range of candidate lane assignments.

Normalization using $(\frac{d(s)-d_{min}}{d_{max}-d_{min}})$ thus scales the delay term to the unit interval. Similar min–max normalization is recommended in multi-objective optimization to remove the influence of different units. Also, for each configuration s, the total expected crash frequency (for each slot) is E(s) = $\sum_i E_{i,slot}$ where $E_{i,slot}$ is given by Eq. (14). The quantities E_{min} and E_{max} are obtained by computing E(s) for all feasible lane states in the current slot and taking, respectively, the minimum and maximum of these totals. The normalized term $\frac{E(s)-E_{min}}{E_{max}-E_{min}}$ therefore ranges from 0 to 1.

The inclusion of ηI_{change} prevents oscillations, meaning frequent back-and-forth lane-state changes (e.g., toggling between one and two lanes on successive slots) that may cause operational instability, driver confusion, or implementation inefficiency. From an engineering perspective, oscillation refers to a control policy that repeatedly alternates between states without achieving a stable pattern, resulting in unrealistic or impractical operation. To further enhance robustness, a priority rule is imposed: any arm experiencing LOS F for multiple consecutive slots automatically receives priority for additional lanes until its level of service improves. This ensures that critical congestion is addressed promptly, while the switching penalty ensures that such adjustments remain stable once improvement is achieved. It should be noted that this acceptance criterion defines an explicit operational analysis domain rather than an unconstrained traffic universe. The retained demand scenarios represent operating conditions in which a conventional single-lane roundabout remains functional but stressed, and in which lane-management strategies can be meaningfully compared. Extremely congested regimes—characterized by persistent gridlock and prolonged LOS F under all configurations—were intentionally excluded, as such conditions typically require network-level interventions, geometric redesign, or signalization rather than intersection-scale lane-activation control. Accordingly, the results of this study should be interpreted as conditional on this defined operational envelope and not as universal performance claims under unconstrained oversaturation. The controller selects, at each slot, the configuration s_t that minimizes J(s) subject to the priority rule. This framework represents a multi-objective optimization problem balancing efficiency (delay) and safety (crash risk) under dynamically changing traffic conditions.

Traffic demand scenarios

Accurate and reproducible demand scenarios are essential for evaluating the proposed lane-control strategies. In this study, demand is represented at each one-hour control slot t by a 4×4 origin–destination matrix $M_{O/D}(t) = [Q_{ij}(t)]$, where $Q_{i,j}(t)$ denotes the mean hourly flow entering at arm i and exiting at arm j. The inflow vector is $q(t) = [q_1(t), q_2(t), q_3(t), q_4(t)]$. To generate realistic turning flows for each arm, a three-parameter Dirichlet distribution was adopted for the right (R), through (T) and left (L) turning proportions $\pi_i = (\pi_{i,R}, \pi_{i,T}, \pi_{i,L})$ [30–32].

The Dirichlet density function is:

$$f(\pi_i) = \frac{\Gamma(\alpha_0)}{\Gamma(\alpha_R)\Gamma(\alpha_T)\Gamma(\alpha_L)} \prod_{k\in\{R,T,L\}} \pi_{i,k}^{\alpha_k - 1} \tag{17}$$

where $\alpha_k > 0$, $\alpha_0 = \alpha_R + \alpha_T + \alpha_L$ and $\pi_{i,R} + \pi_{i,T} + \pi_{i,L} = 1$.

The mean and variance of each component are:

$$E[\pi_{i,k}] = \frac{\alpha_k}{\alpha_0}, Var[\pi_{i,k}] = \frac{\alpha_k(\alpha_0 - \alpha_k)}{\alpha_0^2(\alpha_0 + 1)} \tag{18}$$

$(\alpha_R, \alpha_T, \alpha_L) = (1.4, 2.2, 3.2)$ and $Var[\pi_{i,k}] \approx 0.13$ was set, yielding expected right/through/left proportions of 20.6%, 32.4% and 47.0% respectively. These coefficients were chosen because they produce moderate dispersion ($\alpha_0 = 6.8$) and avoid unrealistic extremes: values less than 1 lead to excessive dominance of a single movement, whereas values above 4 overly constrain variability. Wang et al. [33] report that peak-hour traffic volumes on major arteries can increase by approximately 1.3 to 2.0 times compared to off-peak conditions. Meanwhile, Wang et al. [34] demonstrate that the temporal concentration of travel demand in dense urban environments can lead to even higher intensification coefficients, depending on land-use intensity and commuting patterns. Therefore, the selected coefficients fall within the observed experimental ranges and provide a realistic representation of different levels of traffic intensification during peak periods for field demand modeling. Once a Dirichlet vector is sampled for arm i, its components are mapped to downstream arms j=(i+1)mod4, j=(i+2)mod4 and j=(i+3)mod4, respectively. In mapping the Dirichlet

turning proportions to downstream exits, the index *j* identifies the exit arm relative to the entry arm i: j=(i+1)mod4 denotes the next arm in a clockwise direction (right turn), j=(i+2)mod4 the opposite arm (through movement) and j=(i+3)mod4 the preceding arm (left turn). The modulo operation ensures that when the sum exceeds four, the index wraps around (e.g., an entry at arm 4 yields exit at arms 1, 2, and 3), thereby preserving the circular ordering of the roundabout. In other words, the probability $p_{ij}(t)$ that a vehicle entering at arm *i* exits at arm *j* is equal to the Dirichlet component associated with right, through or left turn, and $Q_{ij}(t) = p_{ij}(t) \cdot q_i(t)$. This formulation guarantees non-negativity and that each row of $M_{O/D}(t)$ sums to $q_i(t)$. Conventional roundabouts often exhibit unbalanced approach volumes, with one arm dominating inflow [35, 36]. To model this, the fraction of the design-hour demand assigned to each arm is also drawn from a Dirichlet distribution with parameters $\alpha^{arm} = (2.8, 2.2, 3.2, 2.5)$. These weights were calibrated so that one arm accounts for roughly twice to three times the flow of the smallest arm, reflecting the 2:1–3:1 dominance ratios observed in unbalanced roundabout traffic and simulation studies [37, 38]. Because Dirichlet sampling preserves the total inflow, this approach introduces realistic asymmetry without altering the overall demand level. Traffic demand over the 12-h horizon is modelled by smooth Gaussian-shaped profiles. For each arm *i*, the inflow $q_i(t)$ evolves as [39, 40]:

$$q_i(t) = q_i^{base} + (q_i^{peak} - q_i^{base}) exp\left[-\frac{1}{2}\left(\frac{t-\mu_i}{\sigma_i}\right)^2\right] \quad (19)$$

where t is measured in minutes from the start of the simulation, q_i^{base} and q_i^{peak} are the baseline and peak inflows, μ_i is the peak time, and σ_i controls peak width.

In this study, for each approach, the mean time of the peak was set to $\mu_i = 6$ h (midpoint of the 12-h analysis period) and the standard deviation to $\sigma_i = 1$ h, resulting in a broad bell-shaped curve. These parameters were chosen to represent typical diurnal traffic peaks and can be adjusted to match local traffic data. This formulation ensures continuity in the first derivative of demand, which is desirable for stability in the optimization routine and reflects the approximately bell-shaped profiles observed in empirical hourly traffic counts [41, 42]. The baseline inflow vector q_i^{base} is (420, 390, 440, 410) veh/h, and the peak inflow vector q_i^{peak} is (1220, 1080, 1280, 1120) veh/h. These two vectors are used for each arm of the COM-Roundabout (from Arm 1 to Arm 4). These values yield a peak-to-base ratio of approximately 3:1 and approximate the diurnal increase observed on busy urban approaches (e.g., midday peaks being roughly three times the off-peak volume), while still respecting typical design-hour demands as specified in the HCM. They are intended as representative values; practitioners can adjust them to reflect local counts.

Monte Carlo simulation was employed to ensure robust statistical representation of stochastic traffic demand and to quantify variability across numerous realizations of the $M_{O/D}(t)$ matrices, incorporating Gaussian-shaped temporal profiles and Dirichlet-distributed turning proportions. To generate a large ensemble of plausible traffic states while preserving probabilistic consistency, the total inflow demand is modelled as a Gaussian-shaped function of time. The normal distribution has long been used in traffic modeling to represent desired speeds and travel times; here, it produces a single peak within the 12-h horizon with minimum flows at the start and end. At each minute, the total flow is divided among the four arms, and the proportions of right, through, and left turns on each arm are drawn from a Dirichlet distribution. The Dirichlet distribution generates non-negative probability vectors that sum to one, with expected component values α_k/α_0. This combination enables realistic variations in both total demand and turning behavior, allowing for the estimation of mean performance indicators and their dispersion, which is crucial for reliability-based assessments of dynamic control strategies [43, 44]. For each Monte Carlo sample, an AADT value within the empirical range (20,000–80,000 vehicles/day) was converted to design-hour flows using the factors $\alpha = 0.10$ and PHF = 0.90, in accordance with HCM conventions. Not all randomly generated matrices are retained. To ensure that the scenarios are both demanding and realistic, each Monte Carlo sample of MO/D(t) was simulated under every static configuration. A matrix is accepted only if: a) the intersection control delay remains below 100 s/veh in all configurations and b) fewer than 30% of the one-hour slots experience level-of-service F. The 100-s threshold is twice the HCM criterion for the boundary F, preventing extremely congested cases from dominating the analysis. The 30% limit ensures that the system remains operational for most of the horizon. Exactly 5,000 accepted matrices formed a common demand pool applied identically to all static and dynamic scenarios at every CAV penetration rate (from 0 to 100%), ensuring that performance differences arise purely from control logic rather than stochastic sampling noise.

The integration of Dirichlet-based spatial randomness with Gaussian temporal variation reproduces the essential empirical features of real traffic: compositional dependence among turns, temporal continuity in demand, and bounded variability. This approach yields a statistically consistent yet behaviorally credible foundation for comparing static and dynamic lane-control strategies under heterogeneous demand conditions.

Results and discussion

Dynamic versus static policies

Across the 5,000 traffic demand conditions considered in this research, the four static configurations (Scenario A–Scenario D) of the COM-Roundabout exhibited marked variability in both operational efficiency and safety performance, whereas the dynamic control policy achieved consistently balanced outcomes. As summarized in Table 6, the dynamic per-arm controller delivers a consistently balanced compromise between the four static configurations across the full range of entering flows. The delay and LOS values in the table are obtained from the HCM-based operational models described in Sect. "Measure of effectiveness: capacity and delay estimation". The expected crash frequencies follow the NCHRP-888 leg-level safety framework discussed in Sect. "Safety model", which is applied to the common Monte Carlo demand pool introduced in Sect. "Traffic demand scenarios". Each cell therefore represents a roundabout-wide average over all four approaches for a given total-inflow band, rather than the performance of a single leg. In the low-demand regime (total inflow q(t) = 500 –1500 veh/h), all configurations operate at LOS A and the differences in mean delay are modest. The dynamic policy essentially coincides with the best static layouts in this range: for q(t) = 500–1000 veh/h it matches Scenario B in both delay and expected crashes, and for q(t) = 1000–1500 veh/h it again mirrors the two-entry lanes design. This behavior reflects the optimization logic described in Sect. "Dynamic lane control optimization": when traffic volumes are far from capacity, the controller has little incentive to deviate from simple multi-lane states that already provide very low delays and acceptable crash exposure. Under these conditions, the primary role of dynamic control is to prevent unnecessary lane activations, maintaining a simple geometry while preserving free-flow operations.

Table 6 Comparison of the analyzed scenarios

Total inflow q(t) (veh/h)	Scenario	Mean delay (s/veh)	LOS	Mean expected crashes (crashes/h)
500–1000	Dynamic scenario	3.7	A	2.2E-04
	Scenario A	4.4	A	8.4E-05
	Scenario B	3.7	A	2.2E-04
	Scenario C	4.2	A	1.7E-04
	Scenario D	3.6	A	3.4E-04
1000–1500	Dynamic scenario	4.7	A	3.9E-04
	Scenario A	6.3	A	1.5E-04
	Scenario B	4.7	A	3.9E-04
	Scenario C	5.7	A	2.5E-04
	Scenario D	4.4	A	5.0E-04
1500–2000	Dynamic scenario	7.3	A	4.4E-04
	Scenario A	9.3	A	2.1E-04
	Scenario B	6.1	A	5.6E-04
	Scenario C	8.1	A	3.3E-04
	Scenario D	5.5	A	6.5E-04
2000–2500	Dynamic scenario	13.3	B	4.0E-04
	Scenario A	18.4	C	2.8E-04
	Scenario B	8.2	A	7.4E-04
	Scenario C	13.4	B	4.0E-04
	Scenario D	7	A	7.9E-04
2500–3000	Dynamic scenario	27.1	D	5.3E-04
	Scenario A	49	E	3.5E-04
	Scenario B	12.6	B	9.2E-04
	Scenario C	32.5	D	4.7E-04
	Scenario D	9	A	9.2E-04
3000–3500	Dynamic scenario	31.4	D	8.3E-04
	Scenario A	82.9	F	4.1E-04
	Scenario B	27.2	D	1.1E-03
	Scenario C	66.1	F	5.3E-04
	Scenario D	12.2	B	1.0E-03

As the total inflow enters the intermediate range (q(t) = 1500–2500 veh/h), the differences among scenarios become more pronounced. Compared with the single-lane baseline (Scenario A), the dynamic configuration consistently reduces delay—by roughly 20–30% for q(t) = 1500–2000 veh/h and even more once flows exceed 2000 veh/h—while also improving LOS from C to B at q(t) = 2000–2500 veh/h. At the same time, dynamic control remains substantially safer than the fully multi-lane layouts. For instance, in the q(t) = 2000–2500 veh/h band, Scenarios B and D achieve very low delays but exhibit crash frequencies almost twice those of the dynamic and Scenario C cases. This pattern illustrates the intended function of the controller: it activates additional lanes only where and when needed, capturing a large share of the congestion relief associated with Scenarios B and D while limiting the duration and spatial extent of high-exposure multi-lane operation. In the high-demand regime (q(t) = 2500–3500 veh/h), the trade-offs become sharp. Scenario A drifts into LOS E–F with delays above 50 to 80 s/veh, and Scenario C also experiences severe congestion in the highest inflow band. The dynamic configuration, by contrast, achieves delays of approximately 27–31 s/veh and LOS D, reducing the delay of the single-lane design by roughly half while maintaining substantially lower crash frequencies than the permanently widened two-lane scenarios. For 2500–3000 veh/h, the dynamic policy incurs about 2–3 times the delay of Scenarios B and D but reduces their expected crash frequencies by around 40%; for 3000–3500 veh/h, it again sacrifices some delay relative to the most aggressive layouts while lowering predicted crashes by roughly one quarter. These results confirm that the optimization in Sect. "Dynamic lane control optimization" is effectively navigating the delay–safety frontier: when the network approaches saturation, the

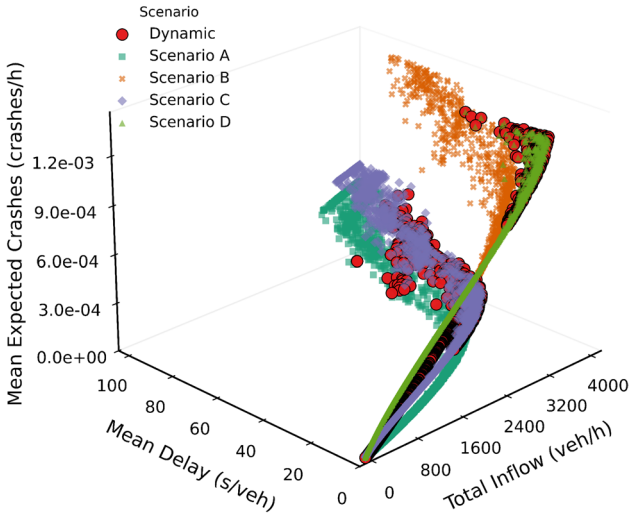

Fig. 2. 3D delay–safety–demand trade-off for the five COM-Roundabout scenarios

controller accepts a moderate performance penalty relative to the minimum-delay designs in order to avoid the highest crash-risk states.

The joint reading of Table 6 and the 3D trade-off plot in Fig. 2 clarifies how the different scenarios of the COM-Roundabout considered populate the delay–safety space. Although Scenarios B and D both provide two entry lanes on each arm, B couples them with a circulating lane, whereas D uses two circulating lanes, so the leg-level SPFs in Sect. "Safety model" assign them different crash elasticities. In the figure, this appears as two distinct "clouds" along the flow axis: the green markers of Scenario B climb more steeply in the crash dimension as total inflow increases, while the purple markers of Scenario D follow a flatter trajectory for comparable mean delays. The dynamic configuration (red spheres) weaves between these static clusters. At low and intermediate flows, it lies close to the low-delay, higher-risk region occupied by B and D, but as volumes approach the upper range it bends toward the safer, higher-delay region near Scenario C and away from the densest green and purple points. Visually, the dynamic cloud traces an interior Pareto-like surface between the extreme "minimum delay" (B/D) and "minimum crashes" (A/C) solutions. This confirms that the COM-Roundabout traffic controller, as formulated in Sect. "Dynamic lane control optimization", does not simply mimic a single static geometry; instead, it actively navigates the 3D delay–crash–flow space, selecting lane configurations that keep the intersection near a balanced frontier of acceptable delay and bounded crash risk across the entire demand spectrum.

Sensitivity analysis

Figure 3a and b illustrate how the dynamic controller responds to changes in the relative weight assigned to safety in the multi-objective function for four representative total inflow levels. Figure 3a shows that, for all total inflow q(t) levels, increasing the safety weight systematically reduces the mean expected number of crashes; however, the strength and shape of this reduction depend on the flow. At q(t) = 1000 veh/h, the curve is almost flat, with only a modest drop in crash frequency when the safety weight exceeds roughly 0.3–0.4, indicating that the system is far from capacity and several lane configurations are both safe and efficient. In contrast, at q(t) = 3000–4000 veh/h the curves exhibit clear "steps": for low safety weights the controller selects aggressively multi-lane states, leading to relatively high crash frequencies; once the safety weight reaches intermediate values (around 0.4–0.6), the controller abruptly switches to safer layouts and expected crashes fall by on the order of 30–50%, after which further increases in the safety weight bring little additional improvement. This piecewise-constant pattern reflects the discrete nature of the control actions: a small change in the safety weight can trigger a complete change of lane configuration when flows are high, and the optimal trade-off between delay and exposure becomes more delicate.

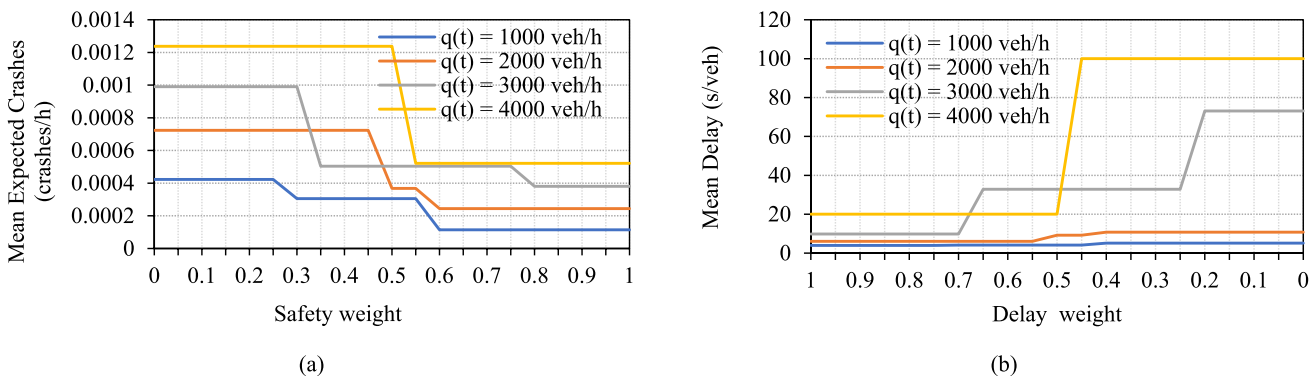

Fig. 3 **a** Sensitivity of expected crashes to the safety weight in the multi-objective controller; **b** Sensitivity of mean delay to the delay weight in the multi-objective controller

Figure 3b shows the mirror image of this behavior in terms of mean control delay. For low safety weights, the controller essentially prioritizes mobility: delays remain close to the minimum achievable for each demand level, particularly for q(t) = 1000 and q(t) = 2000 veh/h, where they stay below about 10 s/veh. As the safety weight increases, the delay curves again exhibit sharp jumps, especially for q(t) = 3000 and q(t) = 4000 veh/h. At these flows, the same thresholds that produce large crash reductions in panel (a) correspond to substantial increases in delay: for example, when safety begins to dominate at q(t) = 4000 veh/h, mean delay jumps from roughly 20 s/veh into the 80–100 s/veh range, and for q(t) = 3000 veh/h it increases from around 10–15 s/veh to more than 30–70 s/veh at the highest safety weights. Together, the two panels make explicit the structure of the delay–safety trade-off embedded in the optimization framework of Sect. "Dynamic lane control optimization": at low traffic volumes, the dynamic controller is largely insensitive to the chosen weights because all feasible states are relatively safe; at high volumes, however, small changes in the safety weight cause the controller to move between qualitatively different operating regimes, offering either low-delay/high-risk or higher-delay/low-risk solutions. This confirms that the COM-Roundabout controller can be tuned by the practitioner to target different positions along the Pareto frontier, depending on whether mobility or safety is regarded as the primary priority for a given intersection and demand level.

To evaluate the robustness of the flow modeling framework, a sensitivity analysis was performed on two fundamental parameters that shape traffic generation. The first is the design-hour factor (α), which determines the overall demand level derived from a fixed AADT, and the second is the peak-to-base ratio of total entry demand (q^{peak}/q^{base}) which characterizes the degree of within-hour demand concentration. Figure 4 illustrates the resulting delay reduction Δd_i (Δd_i = (delay of scenario A—delay of dynamic scenario)/delay of scenario A) of the dynamic scenario relative to Scenario A across the examined parameter combinations. The results reveal a gradual decline in the relative performance gains as demand becomes increasingly peaked, which can be attributed to the reduced operational flexibility available during highly concentrated peak conditions. Conversely, lower values of α, corresponding to lighter overall hourly traffic demand levels, are associated with consistently larger delay reductions. Notably, the dynamic scenario retains a positive delay advantage throughout the entire range of tested parameters, indicating that the observed performance improvements are not sensitive to specific demand assumptions but remain stable under realistic variations in both demand intensity and temporal peaking.

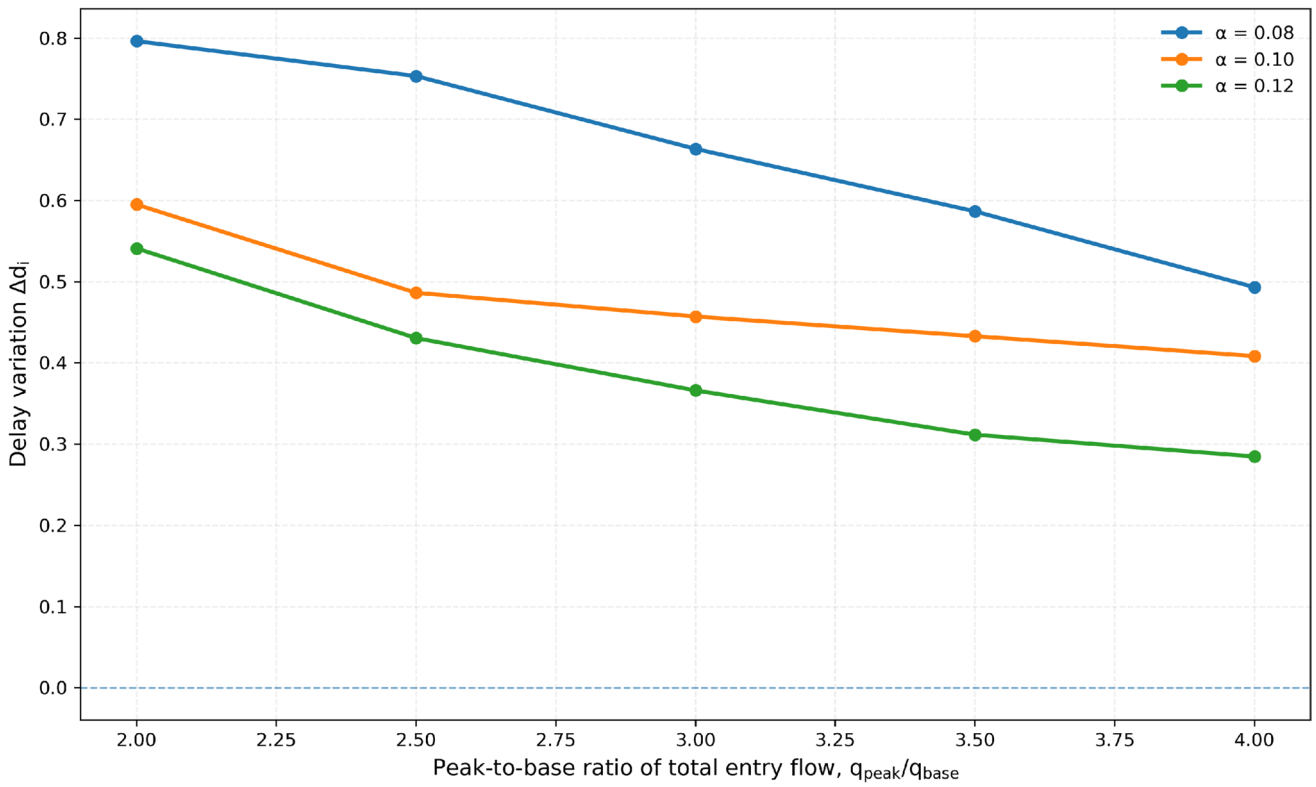

Fig. 4 Sensitivity of delay reduction of the dynamic scenario relative to Scenario A as a function of the peak-to-base ratio of total entry demand (q^{peak}/q^{base}), for different design-hour factors (α), under CAV = 0% conditions

Table 7 Roundabout entry lane capacity model parameters—without CAVs (adapted from [7])

Entry lane type	A	B
One-lane entry, one circulating lane	1,380	1.02×10^{-3}
Two-lane entry, one circulating lane (both lanes)	1,420	0.91×10^{-3}
One-lane entry, two circulating lanes	1,420	0.85×10^{-3}
Two-lane entry, two circulating lanes (right entry lane)	1,420	0.85×10^{-3}
Two-lane entry, two circulating lanes (left entry lane)	1,350	0.92×10^{-3}

Connected and automated vehicles

The adoption of CAVs has the potential to significantly alter the operational and safety outcomes of roundabouts. The presence of CAVs in traffic streams can substantially enhance roundabout capacity due to their ability to maintain shorter and more consistent headways compared to human-driven vehicles. These improvements intensify as the penetration rate of CAVs increases, resulting in significant reductions in delay, queue length, and overall Level of Service (LOS) deterioration. According to the HCM, the entry lane capacity of a roundabout in the presence of CAVs can be expressed as:

$$c_i = f_A \cdot A \cdot e^{-f_B \cdot B \cdot q_{c,i}} \tag{20}$$

where c_i represents the entry capacity adjusted for the CAV share in the total flow, A and B are the intercept and slope parameters, respectively, and $q_{c,i}$ is the conflicting circulating flow rate. f_A and f_B are the adjustment factors applied to A and B to reflect the operational efficiency gained through automation. The baseline parameters A and B depend on the number of circulating and entry lanes (Table 7), while the adjustment factors f_A and f_B vary with the CAV penetration level and lane configuration (Table 8). Together, these parameters quantify the interaction between automation and capacity, allowing direct incorporation of mixed-traffic conditions into performance evaluations. As shown, $f_A > 1$ indicates progressively higher intercepts (and therefore capacity) with increasing CAV percentages, while $f_B < 1$ denotes flatter slopes, representing reduced sensitivity to conflicting flows. This means that with higher automation levels, entry capacity decreases more slowly as circulating flow increases. These factors were incorporated into the present study to update the baseline capacity functions and to simulate mixed-traffic conditions with varying CAV penetration rates.

To evaluate these effects, the HCM CAV adjustment factors were applied to the exponential capacity functions, and the resulting impacts were assessed under varying CAV penetration rates (0–100%) across both static and dynamic lane configurations. The delay estimates reported in this section were obtained using the same stochastic demand scenarios and time-varying inflow profiles described in Sect. "Traffic demand scenarios", with capacity values recalculated through the CAV-adjusted HCM model to ensure methodological consistency. According to Fig. 5, increasing CAV penetration lowers mean delay across all geometric configurations, but the magnitude of this reduction is strongly design-dependent. In the single-lane roundabout of Scenario A, delays climb rapidly with total inflow, and the LOS banding quickly deteriorates to E–F for high demands at low CAV shares. As CAV percentage rises, these high-delay points shrink and shift downward, reflecting shorter effective headways and smoother gap acceptance, but even at high CAV levels, the single-lane design remains the most vulnerable under heavy demand. Scenarios B and D, which provide additional entry lanes and/or circulating lanes, start from a much better operating point: for the same inflows, they occupy LOS A–C predominantly, and the delay surfaces flatten considerably as CAV share increases, indicating that lane supply rather than vehicle technology becomes the dominant constraint. Scenario C, with its adaptive two-lane control, behaves similarly to the full two-lane design and already achieves low delays at zero CAV, confirming that targeted lane activation is very effective in reallocating capacity. Importantly, because the crash-estimation component of the objective function is only valid at 0% CAV, it is removed for CAV shares above zero.

Table 8 Capacity adjustment factors by CAV penetration rate [7]

Proportion of CAVs in traffic stream	1-lane entry				2-lane entry					
	1		2		1		2			
	Circulating lane		Circulating lanes		Circulating lane		Circulating lanes			
					Both lanes		Left lane		Right lane	
[%]	f_A	f_B	f_A	f_B	f_A	f_B	f_A	f_B	f_A	f_B
0	1.00	1.00	1.00	1.00	1.00	1.00	1.00	1.00	1.00	1.00
20	1.05	0.99	1.03	0.99	1.05	0.99	1.03	0.99	1.05	0.96
40	1.12	0.97	1.08	0.96	1.12	0.97	1.08	0.96	1.12	0.93
60	1.22	0.94	1.18	0.92	1.22	0.94	1.18	0.92	1.20	0.87
80	1.29	0.90	1.28	0.89	1.29	0.90	1.28	0.89	1.27	0.84
100	1.35	0.85	1.38	0.85	1.35	0.85	1.38	0.85	1.34	0.80

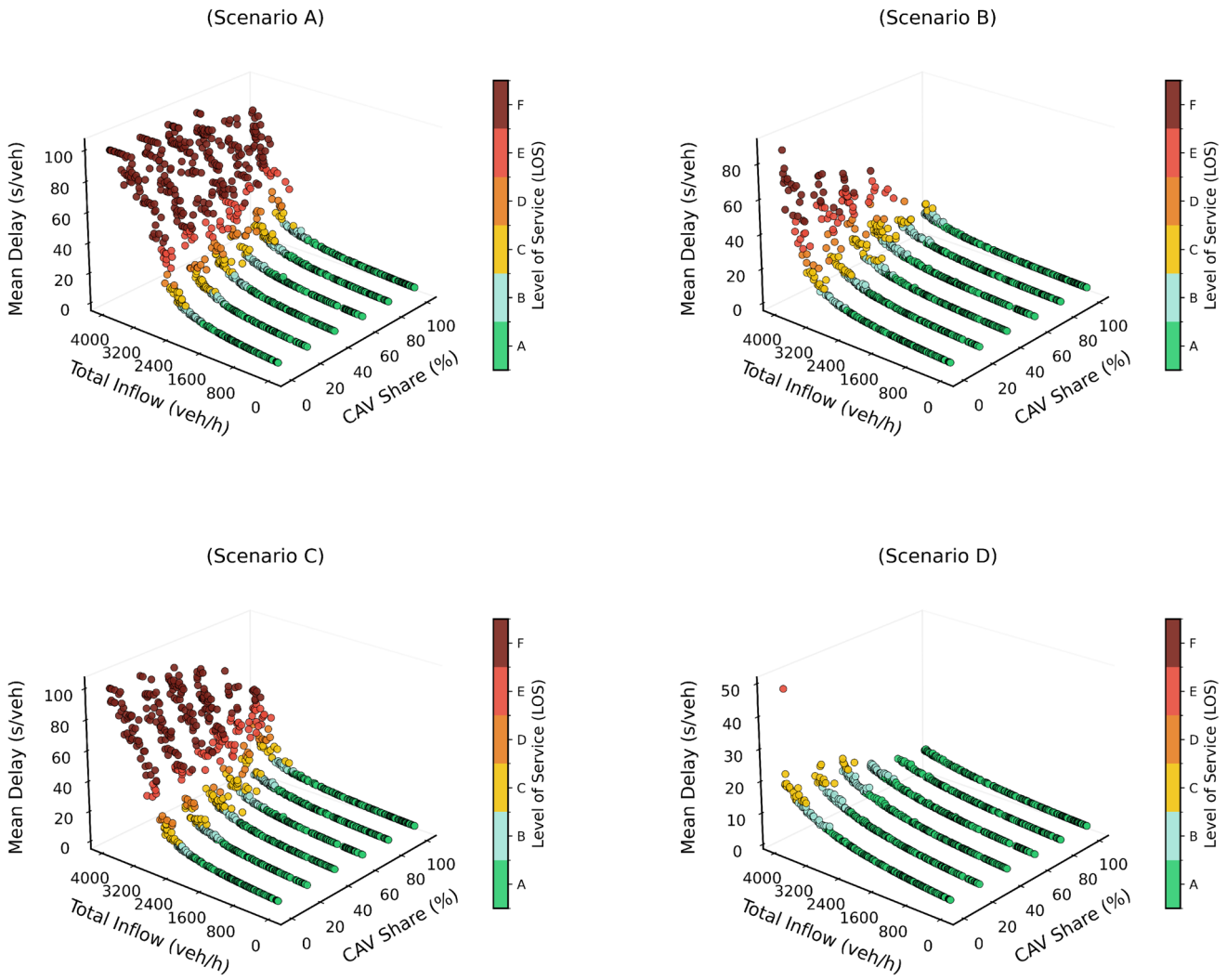

Fig. 5 Mean delay versus total inflow and CAV share for the four static roundabout layouts (Scenarios A–D), with colour-coded points highlighting the resulting level of service

Under this reduced (delay-only) objective, the dynamic control policy converges to the same solution as Scenario D for CAV > 0. Consequently, without considering safety, dynamic and fully two-lane configurations are consistent and offer the least delay among all scenarios, regardless of the CAVs penetration level. This represents a conservative operational assessment that isolates capacity effects while avoiding speculative crash estimates under mixed and automated traffic conditions. However, in the future, by using appropriate formulas to estimate expected crashes with different CAV percentages, different results can be expected for the dynamic scenario. It should be emphasized that the convergence of the dynamic controller to Scenario D under CAV penetration is a direct consequence of the temporary removal of the safety component from the objective function, due to the lack of validated crash-prediction models for automated traffic at roundabouts. Under these conditions, the optimization problem becomes single-objective and delay-minimizing, for which the fully two-lane configuration is mathematically optimal. This behavior does not contradict the balanced trade-off nature of the controller; rather, it reflects a conservative methodological choice that avoids speculative safety modeling. As soon as CAV-specific safety functions become available, the same dynamic formulation will again navigate a multi-objective Pareto frontier, allowing balanced delay–safety solutions under mixed and automated traffic.

Although the present study incorporates CAV penetration through HCM capacity adjustment factors, the crash prediction component of the optimization is restricted to conventional traffic conditions (0% CAV), due to the current lack of empirically calibrated SPF models for mixed or automated traffic at roundabouts. Existing evidence suggests that increasing CAV penetration will reduce crash likelihood by shortening and stabilising headways, reducing speed variance, and improving conflict anticipation through V2V/

V2I communication. However, the quantitative magnitude of these effects remains highly dependent on market penetration, automation level, and cooperative interaction rules between CAVs and HDVs. Future extensions of this framework can incorporate CAV safety using two complementary modeling strategies: (i) modified SPF formulations in which existing NCHRP 888 exposure variables are augmented with automation penetration factors and interaction terms, and (ii) surrogate-safety-based microsimulation approaches (e.g., time-to-collision, post-encroachment time, and deceleration rate to avoid crash), which allow crash risk to be inferred under mixed and fully automated traffic conditions. These methods would enable the dynamic controller to balance safety and delay under CAV-dominated regimes, extending the present formulation beyond its current conservative applicability.

The present formulation assumes reliable and low-latency V2V/V2I communication for cooperative automated vehicles, consistent with current HCM modeling conventions. This idealization simplifies the evaluation of automation impacts but may overestimate achievable performance under real-world conditions where communication delays, packet loss, or partial connectivity can occur. In practice, communication degradation may lead to delayed lane-change execution, reduced platoon compactness, and temporary mismatches between instructed and actual lane usage, potentially increasing transient queues and short-term delay. However, the proposed dynamic controller is inherently robust to such disturbances because control actions are applied over hourly intervals and lane configurations are held constant during each slot. This extended control horizon naturally filters high-frequency communication noise and limits instability due to momentary connectivity losses. Future implementations may further enhance robustness through fallback logic that prioritizes onboard sensing, minimum-hold-time constraints, and decentralized fail-safe lane-use rules, allowing safe operation even under partial communication failure.

Illustrative example

To visualize the real-time operation of the proposed COM-Roundabout traffic controller, Fig. 6 shows a representative 12-h simulation period generated from one of the demand samples considered. The sequence of figures collectively demonstrates how traffic inflow fluctuations propagate through delay and safety responses and how the dynamic lane controller reacts to maintain balanced performance. Figure 6a depicts the time-varying demand profile used in the simulations over the 12-h horizon. The total entering flow (blue curve) and the four arm-specific demands follow smooth, Gaussian-like patterns that rise from a low off-peak level, reach a single dominant peak around the mid-point of the horizon ($t \approx 360$ min), and then gradually decline. While the total inflow attains the highest intensity, the peak time and peak magnitude of each entry differ from the average by about 5–20%, so that some approaches reach their maximum demand slightly earlier or later and with moderately higher or lower volumes than others. This controlled asynchronicity is consistent with observed urban roundabouts, where directional demands rarely surge simultaneously, and it ensures that the case study captures realistic imbalances between approaches. The continuous, unimodal profiles generate a progressive build-up and release of congestion, providing a coherent disturbance against which the static

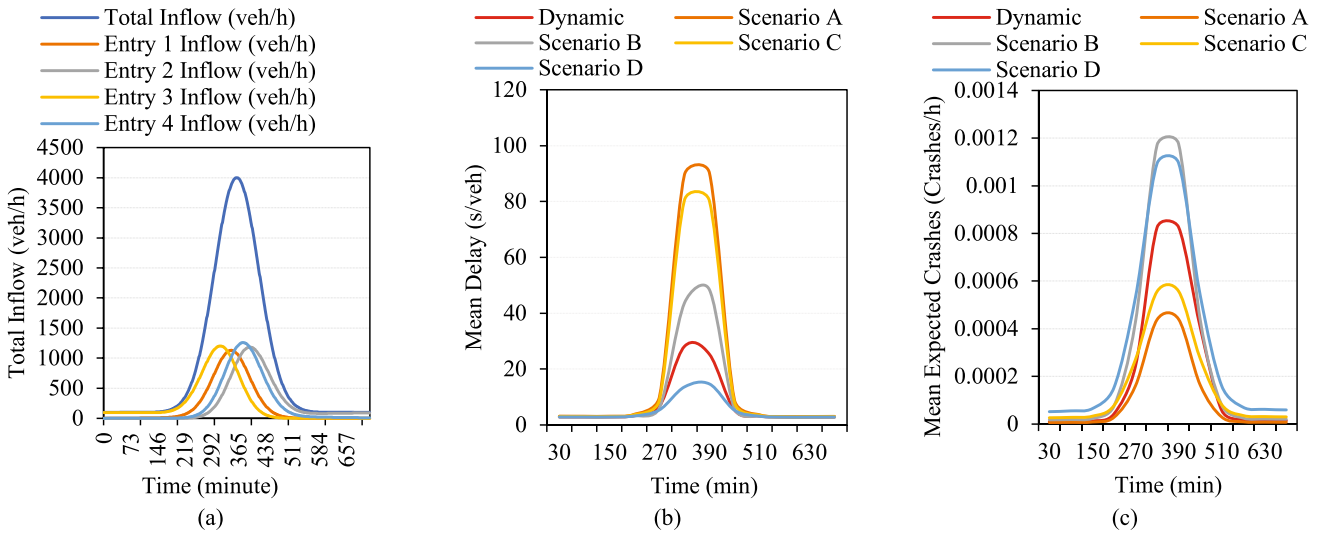

Fig. 6 **a** Temporal variation of total entering flow during a 12-h period; **b** Delay over time for static (A–D) and dynamic configurations; **c** Expected crash frequency

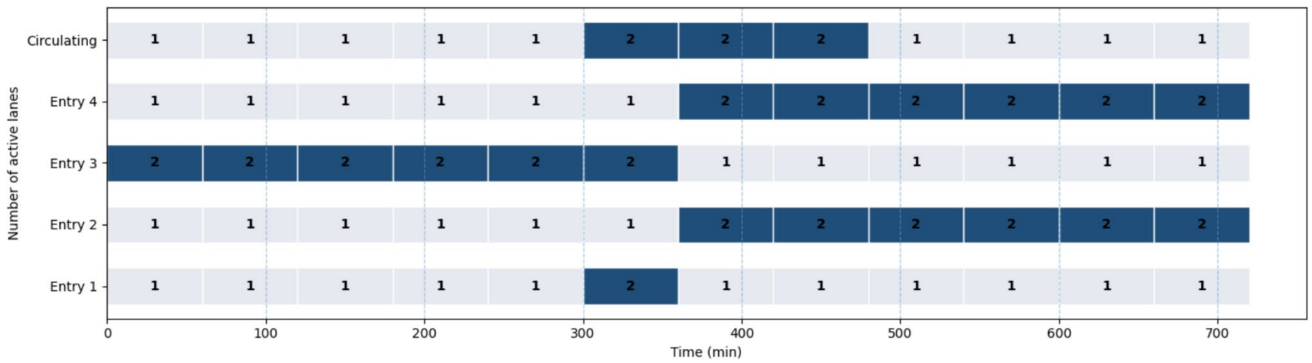

Fig. 7 Dynamic lane-activation schedule over the analyzed 12-h horizon (gray = 1 lane, blue = 2 lanes)

and dynamic lane-allocation strategies can be evaluated over a wide range of operating conditions.

Given the time-varying demand profile in Fig. 6a, b and c show how each configuration translates the same Gaussian-shaped inflow into temporal patterns of delay and safety. As the total entering flow and the four approach-specific demands rise toward their asynchronous peaks (shifted by about 5–20% in both time and magnitude across entries), the mean delay in Fig. 6a remains almost indistinguishable among scenarios during the early low-demand period, then diverges rapidly once total inflow exceeds roughly the mid-range of the profile. The effectiveness of dynamic lane activation depends not only on control logic but also on driver comprehension and compliance. In mixed traffic environments, frequent changes in lane availability can increase cognitive load, especially during transitional periods when drivers must reinterpret lane assignments. Driver adaptation can improve significantly when lane-control states remain stable over minimum hold times and are communicated using standardized, high-contrast overhead lane-use control signals, supplemented by pavement-level LED indicators. For the COM-Roundabout, limiting configuration changes to hourly intervals inherently supports driver learning and reduces uncertainty. The selective activation strategy further minimizes exposure to unfamiliar layouts by modifying only the approaches experiencing demand pressure. Nevertheless, deployment should be accompanied by progressive signage, advance warnings, and public education campaigns to ensure safe behavioral adaptation, particularly during early adoption phases. The single-lane baseline (Scenario A) responds most poorly to the concentrated peak, with delay surging to the highest values and remaining elevated over a relatively long interval. Scenarios B and C offer noticeable relief but still exhibit a pronounced "delay bulge" centred on the time of maximum inflow. The two-lane circulatory layout (Scenario D) compresses this peak, keeping delays substantially lower and shortening the congested period.

The dynamic controller tracks the evolving inflow most efficiently: its curve stays close to the minimum-delay envelope defined by Scenario D, while also reducing the width of the delay peak. This indicates that adaptive lane activation helps the intersection enter and exit congestion more quickly as demand builds and recedes. Figure 6 presents the corresponding evolution of expected crash frequency. Here, the same inflow pulse that drives delay growth leads Scenarios B and D, those relying most heavily on multi-lane operation, to the highest crash peaks, whereas Scenario A remains the safest but suffers from the severe delays seen in Fig. 6b . Scenario C and, especially, the dynamic configuration occupy intermediate positions, with the dynamic policy consistently lowering crash frequency relative to the most aggressive multi-lane designs while retaining much better service than the single-lane case. Taken together, the three figures demonstrate that, under a realistic, single-peak demand pattern with offset approach-specific surges, the dynamic controller is able to follow the demand wave in a more balanced way, mitigating both the intensity and duration of the congestion and avoiding the highest crash-risk states during the critical peak period.

Figure 7 provides a concrete example of the lane-activation schedule generated by the dynamic controller for the demand profile in Fig. 6a, along with the resulting delay and safety patterns in Fig. 6b and c. Over the 12-h horizon, each row shows when one or two lanes are active on the circulating lane and on the four entries (gray = one lane, blue = two lanes). The schedule reveals that the controller does not simply switch to a fully two-lane roundabout during the entire peak; instead, it selectively allocates capacity in time and space. Entry 3, which carries the highest and most persistent flow, is kept on two lanes throughout the day, while Entries 1, 2, and 4 are widened only during the time windows in which their individual inflows approach their Gaussian peaks, with activation periods that reflect the 5–20% shifts in peak time and magnitude across arms. The circulating lane is upgraded to two lanes only between roughly 300 and 480 min, when the total inflow curve reaches its maximum, and then is reverted to a single lane as system-wide demand decays. This pattern explains the behavior observed

in Fig. 6b and c: by activating additional lanes only when and where they are most beneficial, the dynamic strategy captures most of the delay reduction of the fully two-lane configuration while limiting prolonged exposure to high-risk multi-lane states, thereby achieving a more balanced delay–safety trade-off over the full demand cycle.

Discussion

The results of this study highlight that dynamic per-arm lane control developed for the novel smart COM-Roundabout represents a pragmatic middle ground between conservative single-lane operation and aggressive multi-lane static configurations. Whereas single-lane designs (Scenario A) safeguard safety but suffer from chronic congestion, and two-lane designs (Scenarios B and D) maximize throughput but incur substantially higher crash risks, the dynamic controller achieves a balanced compromise. It reduces mean delay with Scenario A, while avoiding much of the crash penalty associated with Scenarios B and D. This demonstrates that adaptive lane allocation can capture many of the operational benefits of multi-lane roundabouts without requiring their permanent exposure to elevated crash risk. The sensitivity analysis confirms that the delay–safety trade-off embedded in the objective function is strongly non-linear and regime-dependent. For low safety weights, the controller systematically prioritizes mobility: delay is kept close to its minimum, especially at a total inflow in the range 3000–4000 veh/h, but expected crashes remain at their highest levels. As the safety weight increases, the system exhibits clear thresholds (around 0.3–0.6, depending on demand) at which the optimal solution switches to safer lane configurations, resulting in reductions in expected crashes of roughly 50–70%, but at the expense of sharp increases in mean delay, particularly under heavy demand. This “knee” in the curves marks a rational compromise region where substantial safety gains can be achieved with moderate degradation in the level of service. From a policy perspective, the safety weight therefore acts as an explicit tuning knob, allowing agencies to position the dynamic controller along the Pareto frontier in line with local priorities, whether emphasizing congestion relief, crash reduction, or an intermediate balance between the two. The analysis of CAVs further strengthens the relevance of dynamic control. Results suggest that CAV penetration amplifies the benefits of adaptive lane management. While static multi-lane configurations continue to deliver the lowest delays under high automation shares. Although dynamic scenario safety analysis for different CAV percentages has not been conducted at present, based on studies, it can be expected that safety will increase with growing automation. On the other hand, dynamic policies require only modest infrastructure (sensors, detection, and lane-control displays), making them implementable in mixed traffic environments and well-positioned to transition into fully automated contexts. From an implementation perspective, the finding that the dynamic controller implements small state changes over a 24-h horizon and may not change for hours is also relevant for driver adaptation. However, in an unbalanced or emergency situation with high volatility, frequent switching may impose cognitive demands on drivers, necessitating clear and unambiguous lane-control signals, as well as minimum hold times, to prevent confusion. These human factors issues highlight the importance of complementing technical optimization with behavioral research and user acceptance studies. Overall, this research contributes to the growing literature on adaptive roundabout management by combining operational models, safety performance functions, and CAV adjustment factors in a unified optimization framework. It shows that roundabouts, traditionally analyzed under static assumptions, can be reconceptualized as dynamic infrastructures capable of responding to real-time conditions. For policymakers, the findings highlight that investing in adaptive control may deliver congestion relief equivalent to permanent widening but at a fraction of the safety cost. For researchers, the study demonstrates the value of explicitly integrating performance trade-offs into optimization objectives and sets the stage for extensions that incorporate environmental metrics, multimodal users, and more complex geometries. The proposed COM-Roundabout controller is conceptually related to broader adaptive traffic management strategies but differs in actuation mechanism and operational envelope. Signalized roundabouts and adaptive signal control approaches regulate priority through signal phasing and can be effective under oversaturation or heavy pedestrian demand; however, stop control and phase constraints may reduce the inherent yield-based safety/efficiency advantages of roundabouts in moderate demand regimes [45–47]. By contrast, dynamic lane-use control reallocates available road space in response to demand while preserving uninterrupted flow where feasible [21, 48]. Within this landscape, COM-Roundabout can be interpreted as an intersection-scale extension of dynamic lane-use control: rather than changing signal priority or imposing stops, it selectively activates entry and circulating lanes to shift capacity toward the approaches experiencing demand pressure. This makes it particularly suitable as a transitional strategy for mixed traffic and for future CAV environments, where actuation can increasingly rely on direct in-vehicle guidance while maintaining conventional signing for HDVs.

Conclusions

This study introduced and evaluated a dynamic per-arm lane-control framework for the novel smart, self-regulating COM-Roundabout, unifying operational, safety, and automation perspectives within a single analytical simulation platform. By integrating HCM capacity functions, NCHRP 888 crash prediction models, and CAV adjustment factors, the work demonstrated that the proposed smart roundabout can be managed as an adaptive infrastructure rather than a static geometric design. The key contribution lies in showing that dynamic lane allocation provides a measured compromise: it alleviates congestion without fully incurring the crash penalties associated with permanent multi-lane widening. Beyond numerical outcomes, the findings highlight several broader insights. First, COM-Roundabouts are equipped with traffic control systems and are supported by sensing and actuation technologies capable of responding to real-time traffic demand. Second, safety and traffic efficiency (in terms of capacity, delay, LOS) do not trade off linearly: instead, their relationship is marked by thresholds and tipping points, offering policymakers levers for tailoring strategies to local priorities. Third, the integration of CAV penetration scenarios suggests that automation can act as a force multiplier for adaptive lane control, accelerating the reduction of congestion phenomena. These insights reinforce the view that infrastructure design, control logic, and technological adoption are interdependent and must be studied holistically. Looking forward, several research avenues emerge. Field implementation studies are needed to move beyond simulation and assess driver compliance, behavioral adaptation, and communication protocols under real conditions. Safety models should be expanded to include CAVs, crash severity, vulnerable road users, and multimodal interactions, thereby reflecting the complexity of urban roundabouts. Future optimization frameworks could integrate additional dimensions, such as energy use, emissions, equity across user groups, and network-level effects, thereby positioning dynamic lane control within the broader smart mobility ecosystem. Advances in artificial intelligence and reinforcement learning may also enable controllers that learn adaptively from observed traffic, striking a balance between stability and responsiveness. Finally, the synergy between dynamic lane management and emerging mobility technologies, CAV platooning, digital twins, and infrastructure-to-vehicle communication, offers fertile ground for reshaping roundabouts into self-regulating, cooperative infrastructures that can sustain both human-driven and automated traffic.

Major findings of the study

In summary, this study positions dynamic per-arm lane control as a transitional yet forward-looking strategy: it is immediately feasible with current sensing technologies, scalable with automation, and extensible to future multimodal applications at the road intersection level. By reframing the smart roundabout as a dynamic system rather than a static one, the research contributes both methodological innovation and practical pathways toward safer, more efficient, and more resilient road intersections. The conclusions of this study are directly supported by the quantitative results presented in Sect. "Results and discussion". Specifically, under moderate-to-high demand conditions ($q(t) = 2000–3500$ veh/h), the dynamic controller reduces mean control delay by approximately 40–60% relative to the single-lane baseline (Scenario A), while maintaining expected crash frequencies that are 25–45% lower than those observed for permanently widened two-lane configurations (Scenarios B and D). In the highest hourly traffic demand band ($q(t) = 3000–3500$ veh/h), the dynamic configuration achieves LOS D with mean delays of approximately 31 s/veh, compared to LOS F and delays exceeding 80 s/veh for the single-lane design, and reduces expected crash frequencies by roughly 20–30% relative to the most aggressive multi-lane layouts. These quantified outcomes provide the empirical basis for the claims regarding the balanced delay, safety trade-off achieved by the proposed COM-Roundabout controller. The reported performance gains are conditional on the defined operational domain and do not extend to extreme oversaturated regimes that would require network-level or signal-control interventions.

Limitations of the study

The present study relies on analytically calibrated capacity and safety-performance functions and does not incorporate microscopic trajectory-level interactions, pedestrian and cyclist behavior, or empirically validated crash models for mixed and fully automated traffic. In addition, communication between CAVs and infrastructure is idealized, and driver compliance is assumed to be high. These assumptions may lead to optimistic estimates of achievable performance. Future research should integrate surrogate safety metrics derived from microsimulation, field-based pilot deployments, and learning-based adaptive controllers to extend the framework to multimodal and network-level environments. The framework does not model transient within-hour shock dynamics, queue spillback, or exit blocking, and is therefore intended for steady-state operating regimes in which circulating and exit lanes remain undersaturated. The use of a neutral 50/50 lane-split assumption for two-lane entries

may influence absolute delay and crash estimates; however, it preserves internal consistency for relative performance comparisons and should be refined using site-specific turning–lane-use relationships in field implementations.

Research perspectives

Future research on smart roundabouts should move beyond analytical evaluation toward field-deployable, learning-based and network-aware control systems. A first priority is the development of empirical crash and conflict models explicitly calibrated for mixed CAV–HDV traffic, enabling the dynamic controller to incorporate safety objectives under partial and full automation, rather than relying solely on conventional SPFs. In parallel, the one-hour discrete control logic of COM-Roundabout can be extended into continuous-time and predictive frameworks using digital twins and reinforcement learning to anticipate near-term demand evolution, queue spillback, and platoon arrivals, allowing smoother lane transitions and reduced switching penalties. At the network level, COM-Roundabouts should be embedded into corridor-wide coordinated control schemes, where multiple smart roundabouts exchange real-time information and jointly optimize delay, safety, and emissions. Additional research should integrate environmental and equity objectives, including CO_2 emissions, fuel consumption, and priority handling for public transport and vulnerable road users, thereby transforming COM-Roundabouts into multi-objective sustainability hubs. Finally, large-scale pilot deployments are essential to investigate driver compliance, communication reliability, cyber-security, and human–machine interaction, ensuring that the proposed adaptive geometry can be safely and effectively transferred from simulation to real urban environments.

Funding Open access funding provided by Università degli Studi di Trento within the CRUI-CARE Agreement.

Declarations

Conflict of interest The authors declare that they have no known competing financial interests or personal relationships that could have appeared to influence the work reported in this paper.

Human or animal rights This study did not involve any human participants, animals, or clinical trials. Therefore, ethical approval was not required.

Informed consent Not applicable. This research does not include any human subjects or identifiable personal data.

References

1. Retting RA, Persaud BN, Garder PE, Lord D (2001) Crash and injury reduction following installation of roundabouts in the United States. Am J Public Health 91(4):628–631
2. Elvik R (2017) Road safety effects of roundabouts: a meta-analysis. Accid Anal Prev 99:364–371
3. Gross F, Lyon C, Persaud B, Srinivasan R (2013) Safety effectiveness of converting signalized intersections to roundabouts. Accid Anal Prev 50:234–241
4. Montella A (2011) Identifying crash contributory factors at urban roundabouts and using association rules to explore their relationships to different crash types. Accid Anal Prev 43(4):1451–1463
5. Guerrieri M, Khanmohamadi M (2025) COM-Roundabout: the first smart commutable and self-regulating roundabout for HDVs and CAVs. Int J Transp Sci Technol. https://doi.org/10.1016/j.ijtst.2025.04.003
6. Almutairi A, Yi P, Owais M (2024) New approach for estimating intersection control delay from passive traffic sensors at network level. IEEE Access 12:2882–2900. https://doi.org/10.1109/ACCESS.2024.3349499
7. Transportation Research Board (2022) Highway capacity manual (7th ed.): a guide for multimodal mobility analysis. National Academies Press, Washington, DC
8. Transportation Research Board (2018) NCHRP research report 888: development of roundabout crash prediction models and methods. National Academies of Sciences, Engineering, and Medicine, Washington, DC
9. Hasan T, Abdel-Aty M (2024) Short-term safety performance functions by random parameters negative binomial–Lindley model for part-time shoulder use. Accid Anal Prev 199:107498
10. Manuel A, De Barros A, Tay R (2020) Traffic safety meta-analysis of reversible lanes. Accid Anal Prev 148:105751
11. Khattak ZH, Smith BL, Fontaine MD, Ma J, Khattak AJ (2022) Active lane management and control using connected and automated vehicles in a mixed traffic environment. Transp Res C Emerg Technol 139:103648
12. Reinolsmann N, Alhajyaseen W, Brijs T, Pirdavani A, Hussain Q, Brijs K (2019) Investigating the impact of dynamic merge control strategies on driving behavior on rural and urban expressways: a driving simulator study. Transp Res F Traffic Psychol Behav 65:469–484
13. Talebpour A, Mahmassani HS (2016) Influence of connected and autonomous vehicles on traffic flow stability and throughput. Transp Res C Emerg Technol 71:143–163
14. Xu Z, Wang X, Wang X, Zheng N (2025) Safety validation for connected autonomous vehicles using large-scale testing tracks in high-fidelity simulation environment. Accid Anal Prev 215:108011
15. Li W, Rios-Torres J, Wang B, Khattak ZH (2024) Experimental assessment of communication delay's impact on connected automated vehicle speed volatility and energy consumption. Commun Transp Res 4:100136

16. Severino A, Pappalardo G, Trubia S (2021) Safety evaluation of turbo roundabout considering autonomous vehicles operation. Arch Civ Eng 67(1):439–460
17. Ye L, Yamamoto T (2019) Evaluating the impact of connected and autonomous vehicles on traffic safety. Phys A Stat Mech Its Appl 526:121009
18. Wang Y, Hu Z, Lu Z, An Q, Wen X (2025) Modeling proactive effects of connected autonomous vehicles on urban traffic in adverse weather. Simul Model Pract Theory 144:103193
19. Kuhn B, Balke K, Wood N, Colyar J (2017) Active traffic management (ATM) implementation and operations guide (FHWA-HOP-17-056). Federal Highway Administration.
20. Ben-Akiva ME, Koutsopoulos HN, Mishalani RG, Yang Q (1997) Simulation laboratory for evaluating dynamic traffic management systems. J Transp Eng 123(4):283–289
21. Wollenstein-Betech S, Paschalidis IC, Cassandras CG (2022) Optimizing lane reversals in transportation networks to reduce traffic congestion: a global optimization approach. Transp Res C Emerg Technol 143:103840
22. Mohebifard R, Hajbabaie A (2022) Trajectory control in roundabouts with a mixed fleet of automated and human-driven vehicles. Comput-Aided Civ Infrastruct Eng 37(15):1959–1977
23. Guerrieri M, Khanmohamadi M (2025) Innovative smart and self-regulating roundabouts. Transp Telecommun 26(4):315–324
24. Miqdady T, de Oña R, Casas J, de Oña J (2023) Studying traffic safety during the transition period between manual driving and autonomous driving: a simulation-based approach. IEEE Trans Intell Transp Syst 24(6):6690–6710
25. Wang C, Xie Y, Huang H, Liu P (2021) A review of surrogate safety measures and their applications in connected and automated vehicles safety modeling. Accid Anal Prev 157:106157
26. Owais M, Abulwafa O, Abbas YA (2020) When to decide to convert a roundabout to a signalized intersection: simulation approach for case studies in Jeddah and Al-Madinah. Arab J Sci Eng 45(10):7897–7914. https://doi.org/10.1007/s13369-020-04479-6
27. Guerrieri M (2024) Total capacity and LOS estimation of innovative and conventional roundabouts through macroscopic fundamental diagrams. Transp Res Interdiscip Perspect 27:101232
28. Mauro R (2010) Calculation of roundabouts: capacity, waiting phenomena and reliability. Springer, Berlin/Heidelberg
29. Sun D, Elefteriadou L (2014) A driver behavior-based lane-changing model for urban arterial streets. Transp Sci 48(2):184–205
30. Krueger R, Vij A, Rashidi TH (2018) A Dirichlet process mixture model of discrete choice. *arXiv preprint*, arXiv:1801.06296.
31. Li Y, Chen Y, Bao J, Xing L, Tang J, Dong C et al (2023) A modified latent Dirichlet allocation topic approach for driving style exploration using large-scale ride-hailing GPS data. J Adv Transp 2023:1–18
32. Reisi Gahrooei M, Work DB (2015) Inferring traffic signal phases from turning movement counters using hidden Markov models. IEEE Trans Intell Transp Syst 16(1):91–101
33. Wang X, Fan T, Li W, Yu R, Bullock D, Wu B et al (2016) Speed variation during peak and off-peak hours on urban arterials in Shanghai. Transp Res C Emerg Technol 67:84–94
34. Wang S, Yu D, Ma X, Xing X (2018) Urban traffic demand distribution and correlation between traffic flow and built environment based on detector data and POIs. Eur Transp Res Rev 10(2):50
35. Guardiola JH (2020) The spherical-Dirichlet distribution. J Stat Distrib Appl 7(1):6
36. Lin J (2016) On the Dirichlet distribution. Department of mathematics and statistics, Queen's University. (Technical report/lecture notes).
37. Akçelik R (2004) Roundabouts with unbalanced flow patterns. In: Proceedings (Paper/Report No. 41). (Conference/technical publication).
38. Transportation Research Board (2010) NCHRP report 672: roundabouts—an informational guide, 2nd edn. NCHRP/FHWA/TRB, Washington, DC
39. Oh SD, Kim YJ, Hong JS (2015) Urban traffic flow prediction system using a multifactor pattern recognition model. IEEE Trans Intell Transp Syst 16(5):2744–2755
40. Zhao J, Sun S (2016) High-order Gaussian process dynamical models for traffic flow prediction. IEEE Trans Intell Transp Syst 17(7):2014–2019
41. Briand AS, Côme E, El Mahrsi MK, Oukhellou L (2016) Mixture model clustering approach for temporal passenger pattern characterization in public transport. Int J Data Sci Anal 1(1):37–50
42. Verma T, Sirenko M, Kornecki I, Cunningham S, Araújo NAM (2021) Extracting spatiotemporal commuting patterns from public transit data. J Urban Mobil 1:100004
43. Deng W, Lei H, Zhou X (2013) Traffic state estimation and uncertainty quantification based on heterogeneous data sources: a three detector approach. Transp Res B Methodol 57:132–157
44. Wang R, Work DB, Sowers R (2016) Multiple model particle filter for traffic estimation and incident detection. IEEE Trans Intell Transp Syst 17(12):3461–3470
45. Ghanim M, Kharbeche M, Hannun J, Hannun J, Shamiyeh K (2020) Safety and operational performance of signalized roundabouts: A case study in Doha. Procedia Comput Sci 170:427–433
46. Tracz M, Chodur J (2012) Performance and safety roundabouts with traffic signals. Procedia Soc Behav Sci 53:788–799
47. Qadri SSS, Gökçe MA, Öner E, Gökçe EG (2019) Analysis of various scenarios to mitigate congestion at a signalized roundabout using microsimulation. In: 2019 innovations in intelligent systems and applications conference (ASYU), pp 1–6. IEEE.
48. Levin MW, Boyles SD (2016) A cell transmission model for dynamic lane reversal with autonomous vehicles. Transp Res C Emerg Technol 68:126–143